ABSTRACT

Title of thesis: AUTOMATIC OPTIMIZATION METHODS FOR PATIENT-SPECIFIC TISSUE-ENGINEERED VASCULAR GRAFTS

Rachel Hess
Master of Science, 2020

Thesis directed by: Professor Mark Fuge
Department of Mechanical Engineering

Surgical intervention is sometimes necessary in cases of Coarctation of the Aorta (CoA). The post-repair geometry of the aorta can result in sub-optimal hemodynamics and can have long-term health impacts. Patient-specific designs for tissue-engineered vascular grafts (TEVGs) allow greater control over post-repair geometry. This thesis proposes a method for automatically optimizing patient-specific TEVGs using computational fluid dynamics (CFD) simulations and the ANSYS Fluent adjoint solver. Our method decreases power loss in the graft by 25-60% compared to the native geometry. As patient-specific graft design can be challenging due to incomplete or uncertain flow and geometry data, this thesis also quantifies the robustness of the optimal designs with respect to CFD boundary conditions derived from imaging data. We show that using velocity conditions that deviate by more than 20% of the measured peak systolic velocity, our method produces grafts with deviations on the order of 5% in predicted power loss performance. Lastly, as one way to accelerate the optimization process, we demonstrate and compare how some

established machine learning models (K Nearest Neighbors and Kernel Ridge Regression) predict reasonable starting points for an optimizer on a 2D bifurcated pipe dataset.

AUTOMATIC OPTIMIZATION METHODS FOR PATIENT-SPECIFIC TISSUE ENGINEERED VASCULAR GRAFTS

by

Rachel Hess

Thesis submitted to the Faculty of the Graduate School of the
University of Maryland, College Park in partial fulfillment
of the requirements for the degree of
Master of Science
2020

Advisory Committee:
Professor Mark Fuge, Chair/Advisor
Professor Axel Krieger
Professor Shapour Azarm

Acknowledgments

First and foremost, my thanks go to my advisor Dr. Mark Fuge for his guidance and mentorship. I'd also like to thank Dr. Axel Krieger, Dr. Narutoshi Hibino, and Dr. Laura Olivieri for sharing their expertise, and Dr. Yue-Hin Loke and Paige Mass for work that made this thesis possible. Thanks as well to my fellow students Seda Aslan, Byeol Kim, and Nicholas Chiu for helpful discussions regarding this work.

Above all, I want to thank my parents and siblings for their encouragement over the years and my wife Sarah for her unwavering support.

Thanks as well to the National Institutes of Health for funding that made this work possible.

Table of Contents

List of Tables

List of Figures

Chapter 1: Introduction

The goal of this thesis is to develop an automatic method for designing hemodynamically optimized patient-specific tissue-engineered vascular grafts (TEVGs) for aortic arch repair. Such repairs are often necessary to address congenital heart disease (CHD). CHD causes roughly 4,000 deaths annually in the United States, more than any other type of congenital anomaly [1, 2]. Though surgical repairs have become more successful over time, long-term morbidities have been extensively documented and linked to the difficulty of optimally reconstructing the aortic arch geometry during surgery [3]. This difficulty exists because traditional non-TEVG graft materials do not provide much geometric flexibility on a per-patient basis, thus making it difficult to design shapes that minimize long-term morbidities.

To get around this difficulty, new TEVG manufacturing methods can construct a graft by electrospinning a biodegradable nanofiber about a 3D-printed mandrel whose shape can be designed to optimize a patient's hemodynamics [4]. The TEVG provides a scaffold for the body to form optimally-shaped native endothelial tissue. The new tissue can grow naturally, which is hypothesized to remove the need for future surgeries to replace conventional grafts as young patients grow. The optimized shape is hypothesized to reduce the severity or incidence of long-term morbidities

linked to aorta shape. The automatic design method presented here aims to reduce the cost and time necessary to design patient-specific TEVGs.

This thesis proposes a method for designing optimal patient-specific tissue-engineered vascular grafts, evaluating the method with regard to (1) how sensitive the optimized patient-specific geometries are to uncertainties in the patient boundary conditions such as flow velocities and pressures; as well as (2) how to simplify the complexity of the flow model to permit faster simulation and convergence towards approximately optimal geometry that one can compute in clinically relevant timescales.

This chapter covers the anatomy of the human aorta, the presentation of Coarctation of the Aorta and related congenital heart diseases, and possible advances in treatment using patient-specific tissue-engineered vascular graft designs. This chapter also briefly covers the use of computational fluid dynamics (CFD) in understanding flow in the aorta and in designing grafts. With this context, then chapter concludes by summarizing the specific research questions that the larger thesis addresses.

1.1 Hemodynamics of the Aorta

In a healthy cardiovascular system, blood exits the heart into the aorta, a large artery with several branches responsible for distributing blood appropriately to the upper and lower body as shown in Figure 1.1. In this thesis, we consider only the portion of the aorta comprising the ascending aorta; the transverse aortic

arch; the three branches: the brachiocephalic trunk, the left common carotid artery (LCC), and the left subclavian artery (LSC); and the descending aorta as shown in Figure 1.2.

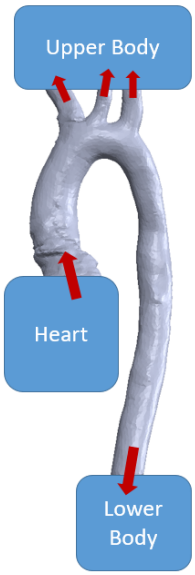

Figure 1.1: The aorta controls the distribution of flow to the upper and lower parts of the body.

The heart receives oxygenated blood from the lungs through the left atrium into the left ventricle. When the left ventricle contracts, blood is forced up into the ascending aorta at high speed where it is then distributed to the upper body through the brachiocephalic, left common carotid, and left subclavian arteries or to the lower body through the descending aorta. These main arteries repeatedly branch until they become capillaries in tissues in various parts of the body, where oxygen is transfered from the blood into the tissues. The deoxygenated blood continues on into the venous system as capillaries rejoin and become larger veins, culminating in the superior vena cava which returns blood from the upper body and the inferior vena cava which returns blood from the lower body. The vena cavae return the

deoxygenated blood to the heart through the right atrium into the right ventricle. From there the deoxygenated blood is pumped into the pulmonary arteries where it becomes oxygenated and then returns through the pulmonary veins to the left atrium, completing the circuit.

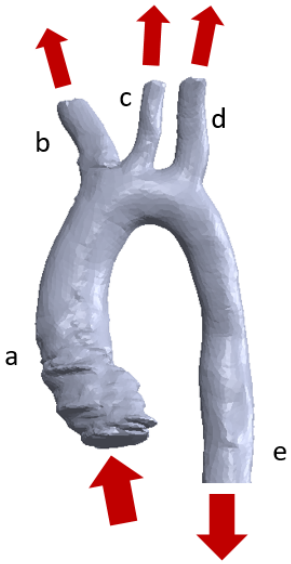

(a) Ascending aorta	
(b) Brachiocephalic trunk	11%
(c) Left common carotid artery	6%
(d) Left subclavian artery	5%
(e) Descending thoracic aorta	78%

Figure 1.2: Typical flow splits to the major arteries and descending aorta for a healthy human, data from [5]

Note that the aorta is responsible for distributing correct proportions of blood to the upper and lower body. In a healthy aorta, the descending branch receives roughly 78% of the flow [5], as shown in Figure 1.2. An example of the pulsatile flow entering the ascending aorta over the course of a single heart beat can be seen in Figure 1.3. Defects in the shape of the aorta can cause poor circulation to certain parts of the body and can lead to significant health problems [6].

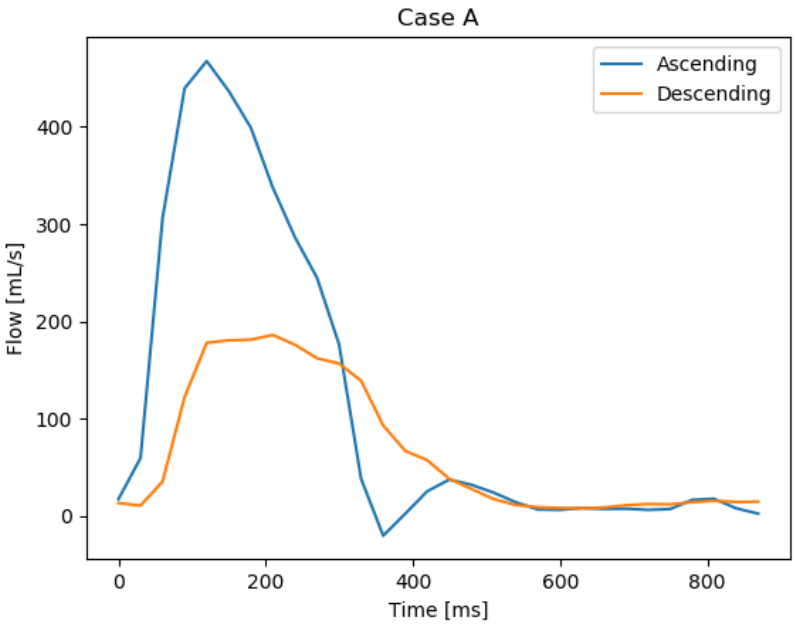

Figure 1.3: Blood flow in the ascending and descending aorta over the course of the cardiac cycle measured using cardiac MRI with contrast for the native geometry of Case A.

1.2 Coarctation of the Aorta

Congenital heart disease (CHD) affects almost 40,000 infants every year in the United States [7]. Of those impacted, approximately one fourth require some form of invasive treatment. Coarctation of the Aorta (CoA), a narrowing of the aorta, is present in 5-7% of CHD cases. Surgical interventions for CHD and CoA sometimes place interposition grafts in the aortic arch that may contain one or more branch. Without intervention, patients with CoA who live past 1 year have an average life span of 34 years [8].

An example of CoA is shown in Figure 1.4. The primary criterion by which CoA is diagnosed is a non-invasively measured supine arm-leg pressure gradient ≥ 20

mmHg, which indicates unhealthy resistance to blood flow through the descending aorta and to the lower body [9]. Such a measurement is likely to precede any imaging procedures. If imaging is done, the ratio of the narrowest diameter of the stenosis to that of the thoracic aorta at the level of the diaphragm is also sometimes considered in diagnosing CoA [3].

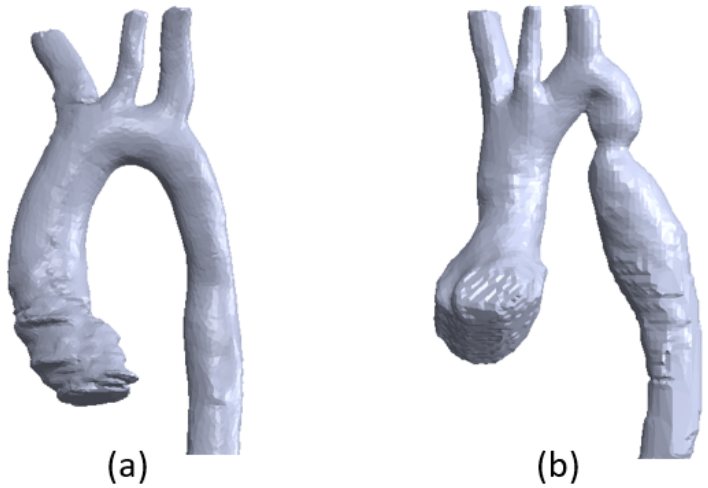

Figure 1.4: Healthy (a) vs. unhealthy (b) thoracic aorta shapes. Note the coarctation distal to the left subclavian artery for the unhealthy aorta.

Patients with CoA sometimes have other cardiac anomalies, such as hypoplastic left heart syndrome, patent ductus arteriosus or ventricular septal defect (VSD). Such cases may require a more complex reconstruction than cases of isolated CoA.

Treatments for CoA

A study of patients with isolated CoA found that 75% of patients underwent surgical procedures consisting of resection with end-to-end anastomosis while 21% of patients underwent resection with tube graft interposition. While the work of

this thesis concentrates on surgical interventions using grafts, other options exist to address CoA. Two transcatheter procedures are used in some cases, particularly when intervention is delayed until adolescence or adulthood [9]. The first intervention, balloon dilation, temporarily places and then inflates a balloon in the aortic arch to stretch the vascular tissue. This induces the tissue to remodel itself into a non-stenotic configuration without requiring a surgeon to implant new grafts to modify the geometry. The downside to balloon dilation is its relatively high stenosis recurrence rates — as high as 80% after a few months in infants [10]. The rate for recurrence in adolescents is lower: 13%, while the recurrence of stenosis for surgical repair in the same study was found to be 0.7% [11].

The second transcatheter intervention places permanent intravascular stents, which consist of a tube whose walls are a mesh-like structure. A surgeon inserts a stent into the location of the stenosis and then expands it to push the wall of the aorta to a larger diameter [12]. After the stent is placed, the vessel takes on a straight cylindrical form as seen in Figure 1.5. As we discuss in Chapter 2, arch shapes that have properties associated with stents (i.e. areas of high centerline curvature at the transitions into and away from the stented area) correlate with long-term morbidities [3].

Grafts

Traditional grafts are generally used when the native tissue shape is extreme enough that resection of the stenosed region leaves too large or too irregular a

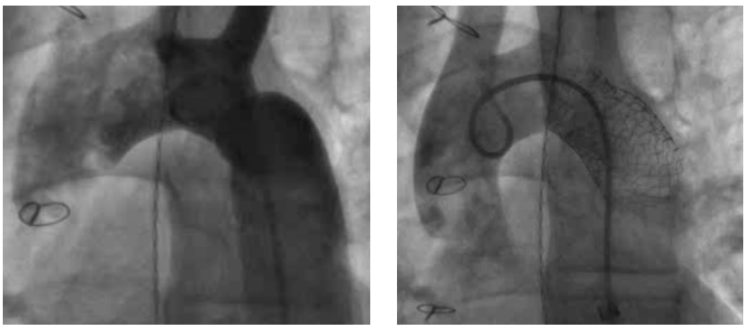

Figure 1.5: Example of repair of CoA using a stent, captured via angiogram. The unrepaired aorta (a) has a coarctation distal to the left subclavian artery. The stented aorta (b) shows an increased diameter in the region of interest.

gap for end-to-end anastomosis or homograft procedures to be practical. These grafts are generally made of tubes of Dacron®(polyester) or polytetrafluoroethylene (PETFE) [13]. A surgeon determines the size and shape of graft to be implanted, relying on experience and intuition. This method does not provide a pre-implementation evaluation of the expected hemodynamics of the repaired aorta. The shape of the graft impacts the hemodynamics of the aorta [3]. If successful, CoA interventions can reduce pressure losses in the aorta and make diameters through the transverse and descending aorta more uniform, ultimately improving patient quality of life and reducing long-term morbidity [6].

One drawback of traditional grafts for use in the aorta is the lack of ability to match the curvature of the aorta, which is typically complex and three dimensional as seen in Figure 1.6. Implanting a traditional graft necessarily adds a segment with little to no curvature with the possibility of sharp transitions into and out of the graft segment. These less-smooth arch shapes have been shown to have negative long-term health implications [3].

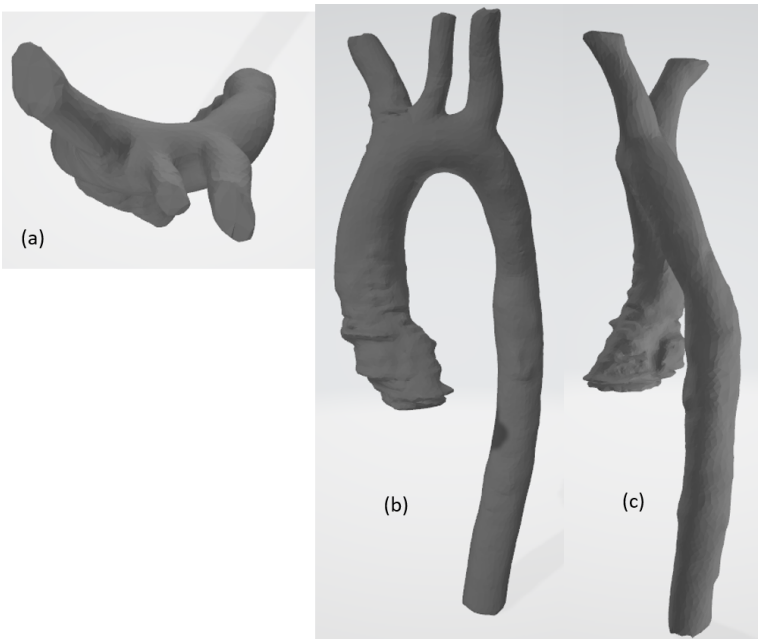

Figure 1.6: A typical aorta viewed from the (a) top (b) front and (c) side. Curvature of the aortic arch is clear in all three dimensions.

Another drawback of grafts is the higher acute health risks associated with the surgical procedure compared to the less-invasive balloon angioplasty or stents. Further increasing these acute health risks is the fact that repeated surgeries are sometimes necessary to replace traditional grafts that are unable to grow with the patient.

It has been hypothesized that TEVGs may be an attractive alternative for some cases that currently are not treated with an interposition graft, as TEVGs do not have the shape constraints or repeated invasive procedure drawbacks of traditional grafts, particularly for pediatric patients [14].

1.3 Using CFD to evaluate aorta hemodynamics

Computational fluid dynamics (CFD) is a type of finite element modeling (FEM) that discretizes the domain of analysis in order to make complex fluid dynamics problems tractable. The Navier-Stokes and conservation equations can be evaluated more simply on each regularly-shaped cell of the mesh than over the whole domain of an organically-shaped aorta, for example [15]. The solutions of neighboring cells are coupled together so that the model closely represents the actual dynamics of the fluid. Conditions can be imposed at the boundary of the mesh, such as an inlet velocity or pressure profile.

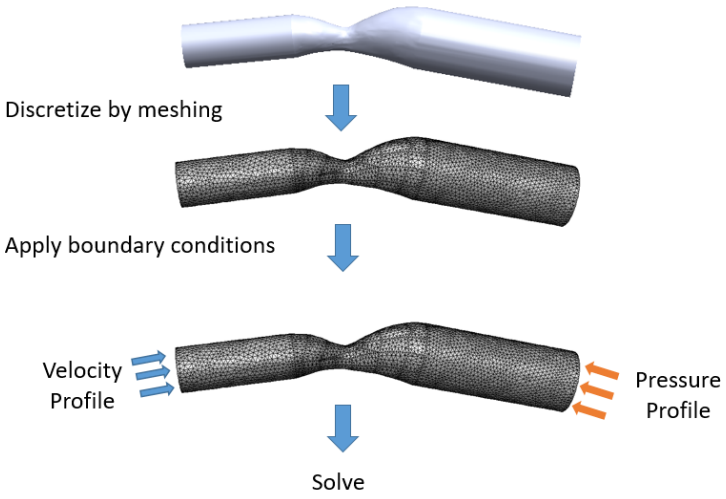

Figure 1.7: Example of discretization and boundary conditions for computational fluid dynamics (CFD)

CFD allows for the evaluation of novel aorta geometries due to grafts, stents, or other procedures without conducting expensive and time consuming in vitro or in vivo tests. Many simulations can be conducted over a variety of geometries and conditions (rigid and non-rigid walls, different velocity profiles due to simulated

exercise, etc.) with a low marginal cost.

If a planned aorta repair can be evaluated via CFD before implantation, design changes can be made and a better post-repair outcome can be expected.

1.4 TEVG technology

Tissue-engineered vascular grafts (TEVGs) are a promising way forward for manufacturing patient-specific graft shapes. A biodegradable nanofiber is electrospun about a 3D-printed mandrel. As long as manufacturing constraints (such as minimum angle between branches) are met, the design of the mandrel can be tailored to produce particular hemodynamics for a particular patient.

Figure 1.8: Pairs of 3-dimensional printed mandrels and electrospun biodegradable grafts. Reprinted from The Journal of Thoracic and Cardiovascular Surgery, Siallagan, D. et al., Virtual surgical planning, flow simulation, and 3-dimensional electrospinning of patient-specific grafts to optimize Fontan hemodynamics, 155(4):1743-1742, 2018, with permission from Elsevier.

The interior of the nanofiber graft may be seeded with cells, and then serves as a scaffold for endothelialization before being resorbed [14]. The nanofiber material is FDA-approved and has shown promising results in sheep and pig models, with the burst pressure and compliance of the TEVG segment matching the surrounding tissue after six months [4]. After several months the graft itself no longer exists; the body simply has new native vascular tissue which can grow with the patient.

Thus in addition to patient-specificity of geometry, TEVGs are also attractive because they would provide a treatment path that requires fewer surgeries than traditional grafts for young patients. Surgeries to implant larger grafts as a patient outgrows the existing graft would be unnecessary. Further benefits include a lower likelihood of thrombosis when compared to traditional graft materials such as Dacron [4].

The TEVG manufacturing process allows for an electrospun graft of arbitrary shape, specific to a single patient. With a wide-open design space, a systematic method is necessary in order to choose a graft shape that produces good hemodynamics. Each patient's aorta is different, as are the boundaries of the 'bad' native tissue. As a result, an automated and flexible design method is desirable.

1.5 Automation of Patient-Specific Graft Design

It has been shown that patients who had successful interventions by the arm-leg pressure gradient standard still see higher incidence of long-term morbidities than the general population, and that the incidence of long-term morbidities correlates with metrics defining the curve of the aortic arch [3].

When the pressure drop criterion for success after repair is lowered from $\leq$ 20 mmHg to $\leq$ 10 mmHg, the incidence of long-term morbidities is significantly lower [9]. This indicates that decreasing the pressure drop as far as possible for a given patient may give that patient the lowest possible likelihood of long-term morbidities. That is, rather than simply replacing stenosed sections of the native

tissue with a simple graft that more closely matches the diameter of the rest of the aortic arch, long-term health benefits may be possible if the effort is taken to design an optimally shaped patient-specific graft.

Recent advances in materials technology make it possible to design an electrospun graft of arbitrary shape, barring manufacturing constraints [4, 16]. We wish to harness the power of CFD and optimization to (quickly and without variance due to engineers' choices) automatically optimize a design.

By establishing a method for quantifying the expected performance of a graft shape, optimization techniques can be applied in order to design patient-specific grafts that have the potential to improve long-term health outcomes for patients with CoA.

In Chapter 2, we describe related work and the state of the art for optimizing vascular grafts. Notably, past work has not addressed practical methods for automatically optimizing aortic grafts or what simplifications to the CFD model one needs to optimize aortic grafts on clinically relevant timescales (ideally, less than a day).

1.6 Research Questions

While the design of patient-specific branching grafts is difficult for a variety of reasons, we can begin the development of a design method that can later be applied to arbitrary portions of the aorta by first solving the problem of optimal graft shape for CoA in the descending aorta.

This thesis addresses the lack of practical patient-specific graft design methods. Specifically, we decompose this problem into the following research questions:

1. "How do we determine optimal patient-specific coarctation repairs?" We investigate this in Chapter 3 by implementing an automatic optimization method based on adjoint shape optimization and compare it to existing surgical practice. In doing so, we uncover insights regarding how to correctly set up gradient-based optimizers on aortic flows as well as common limitations.

   We compare the gradient-based method to a surrogate model method using a parameterized graft shape, and discuss the pros and cons of extending these methods to branching or patch grafts [17].

   The key contribution of this section is a practical method for designing patient-specific grafts for coarctation of the descending aorta, with clear ways to extend the method to more complicated CHD applications.

2. "To what extent are optimal patient-specific coarctation repairs affected by uncertainty in a patient's flow characteristics?" We investigate this in Chapter 4 by conducting a sensitivity analysis of the optimal grafts under a variety of flow conditions relevant to clinical practice. We show that optimal graft shapes are robust even up to large deviations in flow.

   We further investigate the impact of not only the magnitude of flow characteristics from MRI, but also the initial setup of the simplified CFD model. We compare two approaches for establishing the flow profile at the inlet.

The key contribution of this section is an understanding of the robustness of the proposed design method with respect to flow conditions used in the design.

3. "To what extent does machine learning help reduce the computation time needed to produce an optimal graft?" We investigate whether a machine learning approach could provide a 'warm start' for the method described in Chapter 3 or be used as a complete design method, and some of the limitations of that approach.

On five cases of patient coarctations, we demonstrate that the above procedure can produce optimal patient-specific coarctation repair geometry in clinically useful timescales ($\approx$ 1 day). We find that the optimal patient-specific geometries deviate by no more than 2.5% in power-loss even under deviations in as much as 20% in the velocity conditions. This result indicates that optimal patient-specific grafts are robust with respect to flow uncertainties.

Chapter 6 discusses the results and wider impact of the thesis.

Chapter 2: Background and Related Work

This thesis proposes a practical automatic method for designing optimal patient-specific vascular grafts on clinically-relevant time scales, evaluating the method with sensitivity studies and exploring the possibility of 'warm-starting' the optimization [18].

In order to implement this method, we require (1) a paradigm for modeling the hemodynamics of the system (2) a performance objective we wish to optimize (3) a set of design variables to describe the system's geometry (4) an optimization method and (5) an initial design to begin optimizing from.

Work has been done in all five of these areas with respect to the design of internal flow systems, including our particular area of interest: vascular grafts. However, the existing work concentrates on smaller less complicated blood vessels that are simple to parameterize and does not address the uncertainty that exists in the flow and geometry data gathered from cardiac magnetic resonance (CMR) imaging.

This chapter reviews relevant concepts in computational fluid dynamics, graft design optimization, and machine learning.

2.1 Modeling hemodynamics of the aorta

The hemodynamics of the aorta are governed by conservation of mass and conservation of momentum, written as the Navier-Stokes equations

$$\frac{\partial \rho}{\partial t} + \nabla \cdot (\rho \vec{V}) = 0 \tag{2.1}$$

$$\rho \frac{\partial \vec{V}}{\partial t} + \rho(\vec{V} \cdot \nabla)\vec{V} = -\nabla p + \rho \vec{g} + \nabla \cdot \tau_{ij} \tag{2.2}$$

While solving these equations analytically on an organically-shaped domain is impractical if not impossible, discretizing the domain by modeling the aorta using CFD makes the problem tractable [15].The numerical solution of the discretized domain using computational fluid dynamics (CFD) depends on two major factors: the geometry of the domain, and the boundary conditions applied.

Geometry

Aorta geometries can be obtained from cardiac magnetic resonance (CMR) imaging. There is considerable literature on the techniques associated with the capabilities of various CMR techniques and the limitations of post-processing. Resolution of the resulting geometries is limited by the amount of time a patient can spend subjected to ionizing radiation during computed tomography (CT) scans without suffering negative effects, and by the practical limitations on time a patient can be confined to an MRI machine. [19].

Once the aorta geometry has been prepared for modelling by cropping out all but the area of interest, and a mesh has been calculated, boundary conditions can be applied to the inlet and outlets. Material properties can be applied to the walls of the aorta and to the blood. In order to solve the model, some combination of velocity, pressure, and mass or volume flow boundary conditions must then be applied. Time-varying flow data can be obtained from cardiac magnetic resonance imaging (CMR). Pressure data is sometimes available via catheter measurements. In the absence of catheter measurements, cuff pressure measurements can be used to predict pressures in the ascending and descending aorta [20]. Similar studies have focused on using resistance and capacitance models for systemic and pulmonary resistances to flow like the Windkessel model, focusing on predicting velocity and pressure values that would otherwise need to be found invasively [21]. These models have been used to compare pre- and post-repair hemodynamic performance for cases of CoA [22] and to predict aortic dissection in the abdominal aorta [23]. In these cases, accurate representation of hemodynamics is key. However, when considering a CFD model to be used for shape optimization, accuracy can be sacrificed as long as the model allows us to successfully compare designs and determine which design is better according to some in silico metric that does not necessarily have to be accurate to the true measured value of that metric in vivo. As a result, we are free to explore methods that make simplifying assumptions and sacrifice accuracy for computational efficiency.

Several assumptions are commonly made to decrease computation time for models of flow in the aorta. Blood in the aorta can be modelled as an incompress-

ible Newtonian fluid, a generally valid assumption for blood in large blood vessels. Non-Newtonian characteristics of blood are exhibited typically only at low shear rates. [24]. Another common assumption is that of rigid walls, which significantly decreases the complexity of the model and provides reasonably good results [25,26].

2.2 Graft Design Optimization

In the simplest sense, solutions to an optimization problem are found by looking for a point at which the quantity of interest, or the objective, is minimized (for a maximization problem, the negative of the objective is minimized). If the objective J can be described as a function of the design variables $\vec{x}$, and we are able to calculate the gradient ∇J, we can use that information to move in the direction in the design space that most quickly decreases the objective.

In the case of hemodynamics in the aorta, it is not simple to derive design variables that fully describe the geometry of the aorta [3]. Even given those design variables, it would likely be impossible to analytically solve for quantities of interest. That is, we are not able to establish, for example, a compact, analytical objective function $P_{loss}(\vec{x})$ for the total power loss through the system where $\vec{x}$ are all the design variables that define the shape of an aorta, let alone the gradient of that objective function. Given these difficulties, past work has proposed two types of optimization approaches: Gradient-free methods, which forgo attempting to calculate explicit derivatives of the object function, and Gradient-based methods, which use techniques like adjoint simulation to numerically solve for gradient directions at a

given point in the design space.

A variety of optimization methods have been applied to graft design in the past, though none in a manner that lends itself to automatic optimization of patient-specific grafts for CoA on clinically-relevant timescales.

2.2.1 Gradient-free Methods

One strategy involves gradient-free techniques, observing the performance of a set of designs and then iterating the design by making new variations on the best performer from the previous generation.

There are a variety of approaches to design optimization that do not require an explicit gradient function. We first consider an approach that has been applied to similar graft-optimization problems for Fontan repair [27]: that of parameterizing a graft design, then manually modifying those parameters in a systematic fashion and evaluating the new designs using CFD [28, 29]. A very good graft design can be obtained via this method, but the active involvement of an engineer is required. The time required to develop the optimized graft shape can be more than a week, and is susceptible to bias of the engineer's assumptions.

Another approach is to evaluate the objective at various design points and use that data to develop a surrogate function that is easier to optimize. This eliminates the problem of establishing the actual objective function, but still requires establishing the design variables. Such techniques have been applied to TEVG design at the materials-level in order to optimize the mechanical property match between na-

tive tissue, TEVG material, and neotissue that forms on the scaffold [30]. However, the complexity of the problem increases substantially for shape optimization of the graft, which has a higher-dimensional design space.

A third optimization strategy relies on access to a large set of healthy aorta geometries. For example, machine learning techniques can be applied to learn the best geometry that would link a set of inlets to a set of outlets. Clustering techniques have been applied to separate healthy and unhealthy aortas [3], though the parameters found in that study are global in nature and not suited to local shape optimization of patient-specific grafts. During the course of the research outlined in this thesis, a sufficiently large data set was not available to work towards learning optimal repairs. Instead, Chapter 4 demonstrates a proof of concept for generating a data set of optimized two-dimensional (2D) branched pipes.

2.2.2 Gradient-based Methods

Another optimization strategy is to apply a parameterization of the geometry to reduce the number of variables, and then apply a gradient-based method. For example, Dur *et al.* optimized the shape of a coronary artery bypass graft (CABG) by flattening to 2D, parameterizing the geometry with four design variables and then applying a CFD coupled shape optimizer [31]. Quateroni and Rozza described the use of adjoint methods in a 2D CABG case using Stokes flow and defining the boundary of the graft using polynomials, where the weights of the polynomial are used as the design variables [32]. The parameterizations used in these methods tend

to rely on 2D representations that cannot easily be used to reconstruct a 3D graft geometry.

A major competing technique, and the main optimization approach investigated in this thesis, uses gradient information calculated by an adjoint solver [33]. The gradient of the objective function is calculated at each mesh node on the surface of the graft with respect to the position of that same mesh node. This thesis applies an iterative geometry update using the mesh gradients, a method which has not previously been applied to the problem of patient-specific vascular grafts in the aorta, though it has been widely explored in exterior surface flows, such as those of aircraft [34] and in highly idealized 2D coronary artery bypass grafts (CABGs) [32, 35, 36]. These studies fall into two categories that do not apply to the TEVG design problem we are considering: (1) the optimization is performed over a low-dimensional parameterization that would be impractical for our application to grafts for CoA or (2) the problem deals with a two-dimensional idealized geometry for which a surrogate model of the FE solutions can be easily established.

2.3 Effects of Uncertainty on Graft Optimization

All of the above optimization strategies generate graft designs using flow data and geometry data derived from MRI and other imaging methods. Inherent to the imaging process, there is quantifiable uncertainty in the geometry data based on the resolution of the image capture and subsequent segmentation [37]. There is additional unknown uncertainty because the geometry of the aorta is captured

at a single arbitrary point in time during the cardiac cycle. The aorta expands and contracts due to the pulsatile nature of flow exiting the heart. The captured geometry can differ from the aorta's geometry at other points in time by up to 3.3% in terms of diameter [38]. Flow data in the ascending and descending aorta is captured over time, but not all imaging techniques used in the collection of the geometries used in this research make it possible to ascertain which flow data point corresponds to the captured geometry.

This uncertainty about the parameters of the system naturally extends to uncertainty about the result of the optimization. Within what range of input conditions can we claim that the generated graft design is the 'best' design? Would a slight change in input parameters suggest a different graft design? We investigate these questions in Chapter 4.

Another interesting approach is material distribution-based topology optimization, which has been demonstrated for the layout of two-dimensional dual pipe designs [39]. This approach becomes significantly more computationally costly when posed in 3D. Zhang and Liu used a level set method for topology optimization of CABGs [40]. The same paper also shows a method similar to the material distribution method: solid points are seeded in a mostly fluid mesh grid, then the distribution of material is iterated upon until an optimized branched geometry is arrived at. This method is again significantly more computationally expensive in 3D, and does not guarantee a solution that has a sensible i.e. tube-like or water-tight shape.

The methods above that use gradient-free descent rely on an engineer to deter-

mine which variables to include. Parameterizations developed for 2D representations of the aorta cannot be easily extended to 3D. Optimization using adjoints has focused on adjoints of parameterized geometries in 2D, and as a result has the same weaknesses as the gradient-free methods. Additionally, these methods have not focused on graft design for the aortic arch, but rather for CABGs or the abdominal aorta, where geometry of the vessels can be represented well in 2D.

When designing aortic grafts, the approaches above do not suffice. The typical shape of an aorta involves curvature in multiple dimensions as seen in Figure 1.6 and (unlike CABG and abdominal aorta shapes) cannot be represented as a 2D slice or cross-section without losing important features that affect blood flow [3].

A parameterization of the 3D geometry could be employed, but different patients have 'non-optimal' native geometry in different locations. As a result, that parameterization would need to be 'clamped' differently for each patient, and would be difficult to later extend from applications to coarctations in the descending aorta to applications to grafts for more complex CHD cases involving the arch near the brachiocephalic and subclavian arteries.

Therefore the optimization and design methods for CABGs or simplified representations of the aorta are not useful for application to graft design in a clinical setting.

Given these gaps in the literature, the next chapter proposes an automatic patient-specific graft design method that can be practically applied to coarctation of the descending aorta in the current clinical setting. In later chapters we address the question of robustness of the method and possible future extensions of the design

method.

Chapter 3: Pilot Study: Automatic Optimization Method for Aortic Flows

As described in Chapter 2, existing methods for design of vascular grafts fall short of being ready to implement for automatic graft design for coarctation of the aorta. To address that gap, this chapter proposes a method for automatic optimization of graft geometry for coarctation of the aorta. The method's performance is evaluated for five patient cases with respect to the following criteria.

We seek a design method for patient-specific grafts that generates a graft that produces good hemodynamic performance. We want the method to be useful in a clinical setting, where engineers are not generally available. Therefore we wish to automatically generate an optimal patient-specific graft. The methods for graft optimization described in Chapter 2 almost uniformly study 2D configurations, and use a relatively simple parameterization to describe the system's geometry. We want our method to eventually extend to more complex graft shapes on the aortic arch, not just tube-like grafts in the descending aorta. As a result, we want to be able to selectively fix or constrain the geometry of portions of the aorta that we are not planning to modify surgically.

That is, if we parameterized the entire aorta we would perhaps design a 'better'

shape from our optimization. However, it could be impossible to implement because it would call for modifying part of the aorta that is not within or even close to the area that needs to be replaced with a graft. While a sophisticated parameterization method is theoretically feasible, there is not an existing accepted and compact parameterization for aortic repairs. In response, we can consider the adjoint method since it scales more readily to parameterizations of larger dimension. While previous work on graft optimization assumed that adjoint solutions were too computationally expensive, we find this not to be the case for our 3D model of simple coarctation in the descending aorta. Additionally, the mesh-node-level control provided by the optimization method using adjoint sensitivities described in this chapter lets us easily constrain parts of the geometry that we do not want to change.

In summary, there are three criteria we hope to meet with the method outlined in this chapter:

1. **Automatic:** Does not require the active participation of an engineer.

2. **Fast:** Produces a graft design on a clinically useful timescale, i.e. in less than a day.

3. **Robust:** Can be implemented with minimal flow measurement information to avoid invasive procedures that are necessary for a full characterization of the flow parameters.

To handle the third criteria, we develop a method that has simple inputs. The robustness of the method is investigated in Chapter 4.

3.1 Methodology: Adjoint Method

The method developed for optimizing patient-specific TEVGs for repair of CoA is shown in Figure 3.1. In this thesis, we focus only on the processes in red; we do not address specifics relating to CMR data extraction and graft manufacture via electrospinning.

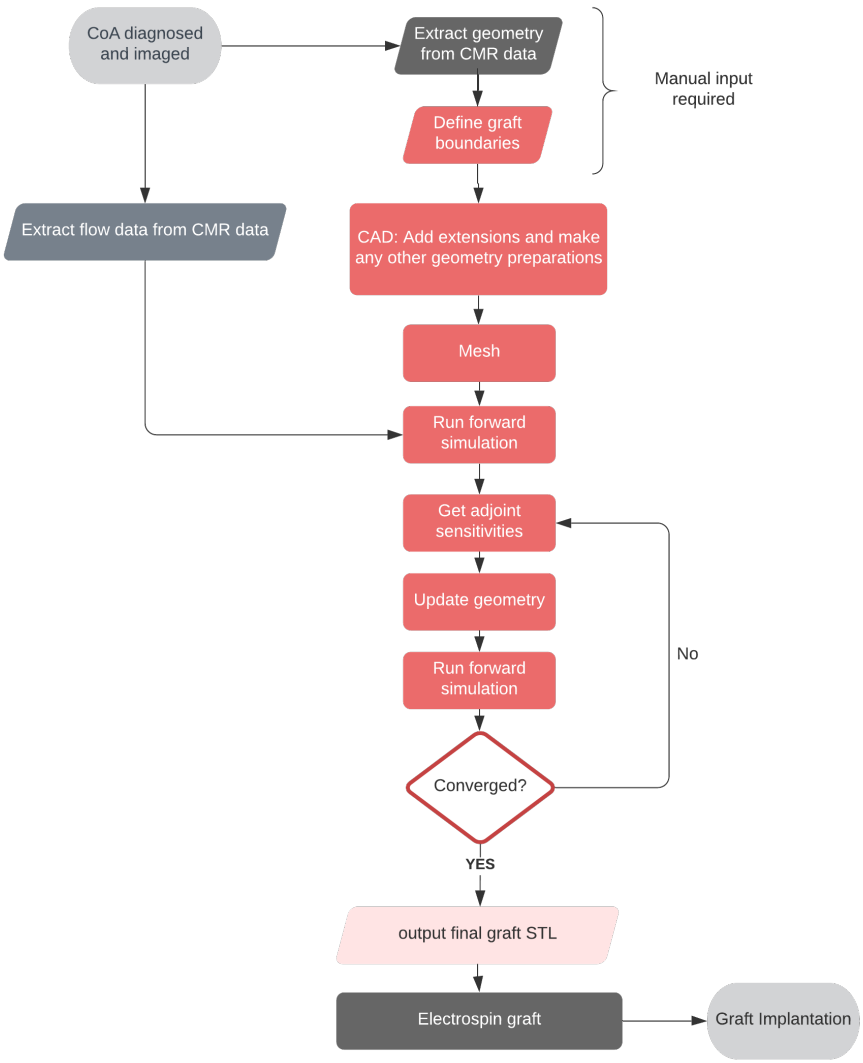

Figure 3.1: Flowchart of the adjoint optimization method.

3.1.1 Geometry setup

We evaluated our optimization method on five pre-repair aorta geometries with coarctations of the descending aorta. For each case, the geometry of the aorta was extracted from CMR imaging data acquired as part of an Institutional Review Board (IRB) approved retrospective study. The geometries can be seen in Figure 3.2. Our clinical collaborators segmented the images to generate the three dimensional model using Mimics (Materialise, Leuven, Belgium). Values for peak systolic flow in the descending aorta were obtained from 4D-Flow MRI.

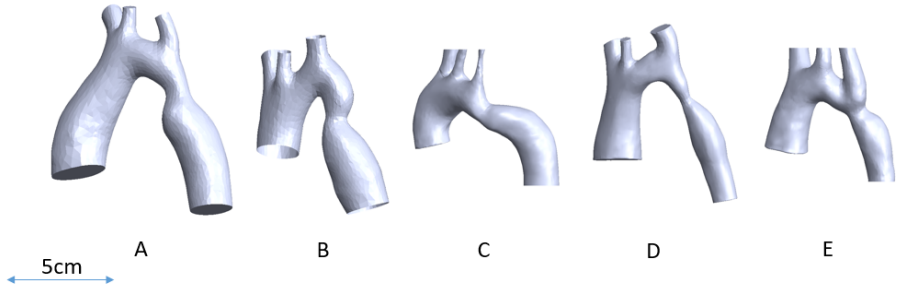

Figure 3.2: The five pre-repair coarctation of the aorta patient geometries studied in this thesis, consistently scaled.

Using the 3D model derived from imaging data, we then identified the portion of the aorta that is to be replaced with a graft using the Vascular Modeling ToolKit (VMTK) [41]. In this work, the choice of graft endpoints was made by an engineer based on visually obvious locations of stenosis in the descending aorta. In practice, a surgeon or cardiologist would define such endpoints by interacting with the software during planning [29]. The flow of the work in the automatic method does not require that the model is defined in this manner. That is, in the future, more complicated cases of coarctation in the aortic arch could be addressed with our design method.

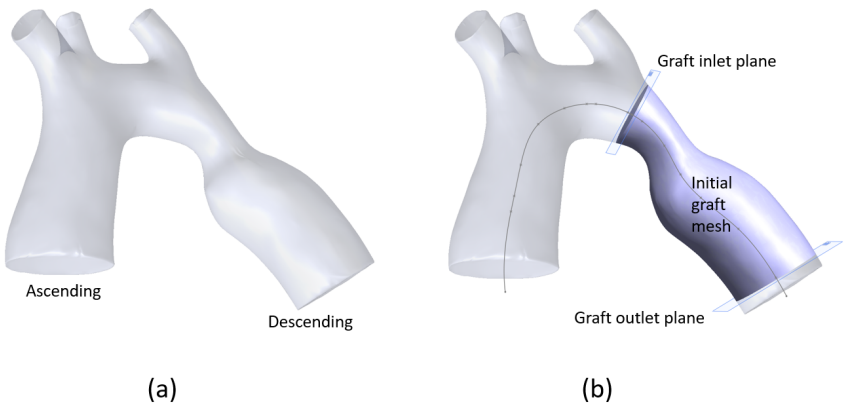

Figure 3.3: A 3D model of an aorta that has been (a) segmented and smoothed, and (b) prepared for graft optimization. The shaded portion becomes the initial graft geometry for the adjoint optimization.

For instance, a surgeon could identify the boundaries of the patch of native tissue that is to be resected using an extension to the current VMTK setup or using an augmented reality tool geared towards medical professionals.

The centerline through the ascending aorta, the arch, and the descending aorta was calculated using VMTK. Points along the centerline were selected as the boundary of the graft region. The 3D model was cropped at those points perpendicular to the direction of flow as shown in Figure 3.3.

Extensions were added to both ends of the graft. The extension at the inlet, along with no-slip conditions imposed on the extensions and graft segment, allows for the development of a realistic flow front of parabolic character at the true graft inlet based on the average velocity applied at the extension inlet. The extension at the outlet prevents our simulation from failing to converge due to reversed flow at the outlet. These modifications were made using Solidworks (Dassault Systèmes,Vélizy-Villacoublay, France). The length of each of the extensions

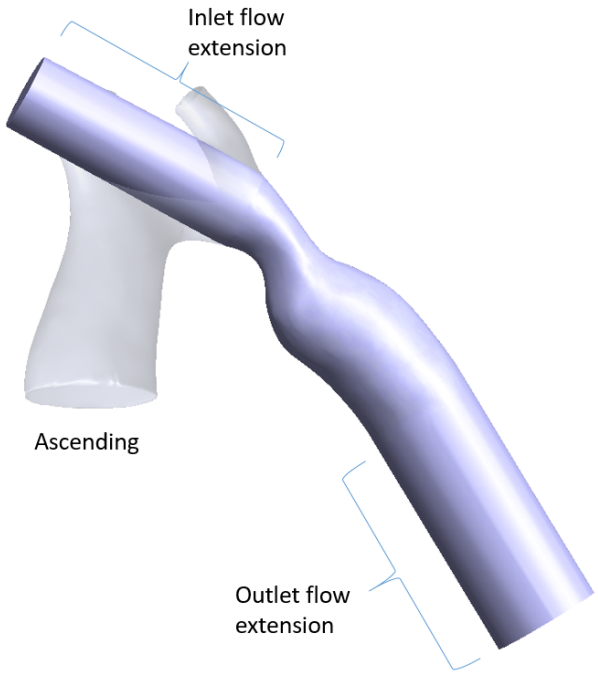

Figure 3.4: A 3D model of the initial mesh with extensions (purple) overlaid with the full aorta model.

was chosen to be approximately five times the effective radius of the larger of the inlet or outlet for each case as seen in Figure 3.4. We found this length to be a good trade-off between simulation time due to increased number of elements and convergence of the objective function (pressure drop) through the system following guidance from industry professionals [42].

The models were meshed using ANSYS Mesh version 19.2 [43] with five layers of inflation elements along the walls of the graft and extensions for finer velocity prediction near the surface, following the setup used in Reymond et al. [44].

3.1.2 CFD Model

ANSYS®Academic Research Fluent version 19.2 [45] was used to solve the 3D Navier–Stokes (equation 3.1) and continuity (equation 3.2) equations for incompressible flow.

$$u \cdot \nabla u + \frac{\nabla p}{\rho} - \nu \nabla^2 u = 0 \tag{3.1}$$

$$\nabla \cdot (\rho u) = 0 \tag{3.2}$$

An average velocity was enforced at the inlet and the outlet pressure was set to 0 Pa. The flow was modeled as steady-state. Blood was assumed to be Newtonian with density $\rho = 1060\ kg/m^3$ and viscosity $\nu = 0.00371\ Pa \cdot s$. The walls of the model were assumed to be rigid. The standard $k - \epsilon$ turbulence model was used due to the Reynolds number $Re > 2100$. A no-slip condition was imposed on the walls of the graft and extensions. All models were considered converged when the residuals for continuity and velocity fell below 10^{-6}.

Adjoint Optimization Algorithm

The mathematics and attractive qualities of adjoint optimization are described in Chapter 2. We describe here our practical implementation of adjoint optimization.

Our optimization approach to the design of patient-specific TEVGs essentially performs gradient descent using gradients provided by the adjoint solver. Specifically, we iteratively calculate the graft mesh node sensitivities with respect to the

performance objective (power loss) and then move each mesh node by an adaptive step size. ANSYS adapts the step size in an attempt to achieve a user-specified objective function change. For simple coarctations with a single inlet and single outlet, minimizing the pressure drop from the inlet to the outlet also minimizes power loss. To calculate the node sensitivities ∇P_{drop} the following automated process is necessary at each step:

- Solve the forward CFD model.
- Solve the adjoint CFD model.
- Calculate the mesh node movements to obtain a target improvement in the objective function.
- Check for errors (e.g. bad skewness or negative-volume cells) and repair the mesh as necessary.
- Finalize the mesh morph and prepare a new forward CFD model.

Adjoint Solver

This work uses the ANSYS Fluent Adjoint Solver to obtain the gradient of the objective function at each node with respect to that node's own position, $\nabla J = \nabla P_{loss}(\vec{x}_i)$ where J is our objective function. During the adjoint simulation run, we provide a target percentage we would like to increase or decrease the objective function by.

Objective Function

As described in Chapter 2, we wish to decrease the power drop through the graft. This is a function of the pressures and flows at the inlets and outlets as seen in equation 3.3.

$$J = \sum_{inlets} Q\left(\bar{p} + \frac{1}{2}\rho \cdot \bar{u}^2\right) - \sum_{outlets} Q\left(\bar{p} + \frac{1}{2}\rho \cdot \bar{u}^2\right) \tag{3.3}$$

where $\bar{p}$ is the average pressure across the inlet or outlet and $\bar{u}$ is the average velocity magnitude on the inlet or outlet.

For the single-inlet, single-outlet structure of these coarctations in the descending aorta, power loss is minimized when pressure drop is minimized. Pressure drop can be directly optimized for using the Fluent adjoint solver. For a more complicated graft, it would be necessary to define the power loss as a function of quantities ANSYS is able to collect gradients for. The power loss is described in equation 3.4 where the volume flow Q is identical at the inlet and outlet, and as a result $\bar{u}_{inlet}$ and $\bar{u}_{outlet}$ vary with the ratio between the inlet and outlet areas.

$$J = Q_{desc}\left(\bar{p}_{inlet} + \frac{1}{2}\rho \cdot \bar{u_{inlet}}^2\right) - Q_{desc}\left(\bar{p}_{outlet} + \frac{1}{2}\rho \cdot \bar{u_{outlet}}^2\right) \tag{3.4}$$

Convergence

The method targets a mesh modification that produces a 5% drop in pressure loss at each optimization iteration. The targeted drop is generally achieved well

during early iterations, giving a smooth curve as seen in Figure 3.5. The design is considered to have converged when the value of the objective function, in this case the pressure drop, converges to 1% of the objective function value at the previous iteration over three adjoint steps.

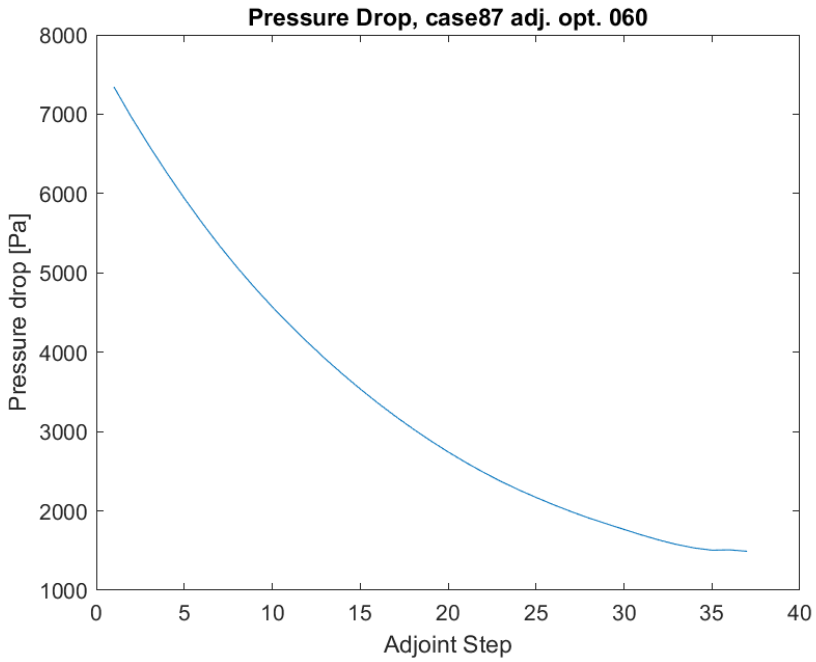

Figure 3.5: An example of convergence of pressure drop through the graft over the adjoint steps.

3.1.3 Traditional Graft Comparison

In order to determine the performance of our method, we wish to compare our grafts to the current standard of care. Post-repair MRI data is not available for all cases, so a method is necessary in order to generate models of the expected post-repair geometries.

We assume that the bounds of the resection are identical, and therefore can use identical inlet and outlet extensions for these traditional graft models and for our

initial models for automatic optimization. To prepare the traditional graft model, these inlet and outlet extensions are kept (preserving the patient-specific inlet and outlet locations, orientations, and profiles) and a tube-like geometry is constructed between in CAD.

Because the inlet generally has a smaller diameter than the outlet, we assume a somewhat-pliable tube graft that is identical in circumference to the outlet at its base and modified by the surgeon to taper to the inlet. A circular segment guideline of is constructed between the inlet and outlet profiles. While specific figures for minimum bend radius (to avoid collapse or folding) of vascular graft materials are not readily available, we assume that the radius of the guideline may not be lower than $10r$, where r is the radius of tubing in use. The inlet-end of the traditional graft is then blended into the inlet extension.

The same boundary conditions are applied to the traditional graft geometries as to the initial forward simulation of the automatic optimization.

3.2 Results

Five patient cases were used to test our adjoint-based method. Measured flow velocities for each case in the descending aorta were between 0.6-3.5 m/s at peak systole as seen in Table 3.1. For the purpose of optimizing the geometries, nominal velocity was considered to be 50% of the measured peak systolic velocity. We show in Chapter 3 that our results and the optimized geometries are not sensitive to this choice.

Case	Peak Systolic Velocity [m/s]
A	2.79
B	3.41
C	2.86
D	0.60
E	2.01

Table 3.1: Flow velocity in the descending aorta at peak systole for the five patient cases, measured by 4D flow MRI.

Using this nominal velocity condition, the optimization method decreased the power loss in the graft by 25-60% as shown in Figure 3.6. We find that our optimizer produces similar results to traditional interposition tube grafts.

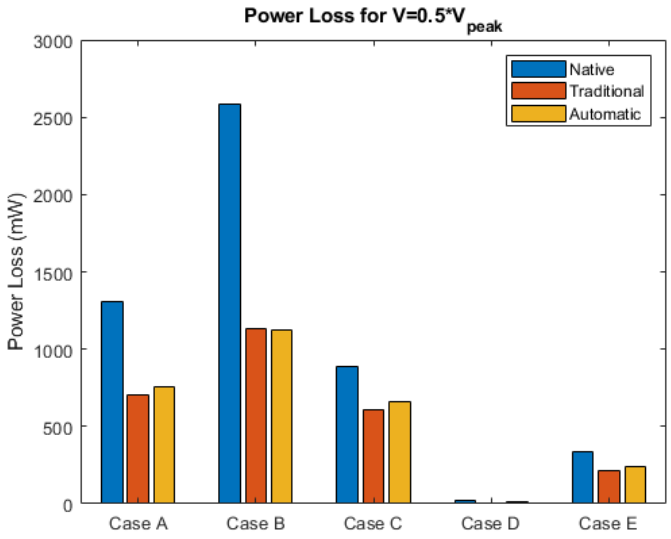

Figure 3.6: Power loss calculated for each initial (pre-repair) graft geometry, for the traditional interposition graft geometry, and for the graft geometry optimized at $V_{in} = 0.5 \cdot V_{peak}$ m/s.

3.3 Methodology: Gaussian Process Surrogate Model

The automatic method outlined above uses adjoint sensitivities calculated with respect to the 3D positions of each node in the mesh. As a result we avoid entirely

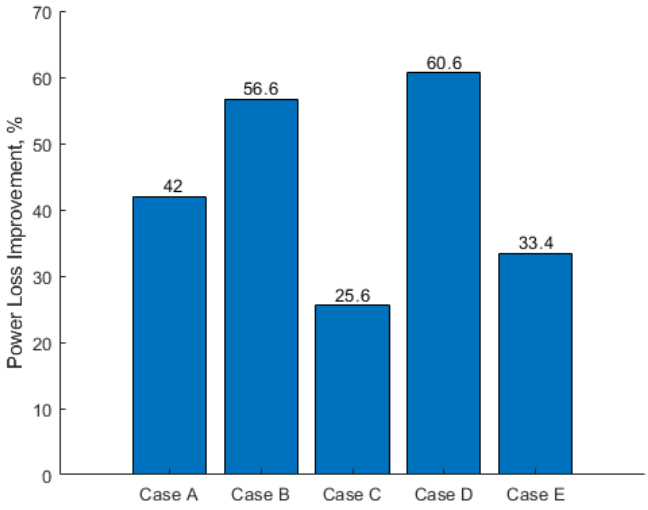

Figure 3.7: Power loss percentage improvement for each case after optimizing at $V_{in} = 0.5 \cdot V_{peak}$ m/s.

the problem of developing a low-dimensional representation of graft geometry. Not needing to establish a parameterization of aorta geometry is an attractive proposition for the eventual goal application of this graft design procedure – patient-specific design of grafts located anywhere in the aorta. However, adjoint-methods can come with their own restrictions based on solver availability, so we wish to compare our approach's performance to that of a different State of the Art method that does not require access to adjoints. Specifically, we briefly explore the use of Gradient-Free Surrogate Model based optimization using Gaussian Processes.

3.3.1 Parameterization for Surrogate Model

The simple tube-like grafts for CoA in the descending aorta that are modeled in this thesis can be represented with only a few design variables. For the purposes of this comparison, we consider points $\vec{x} \in \mathbb{R}^4$. We construct a graft centerline S_g

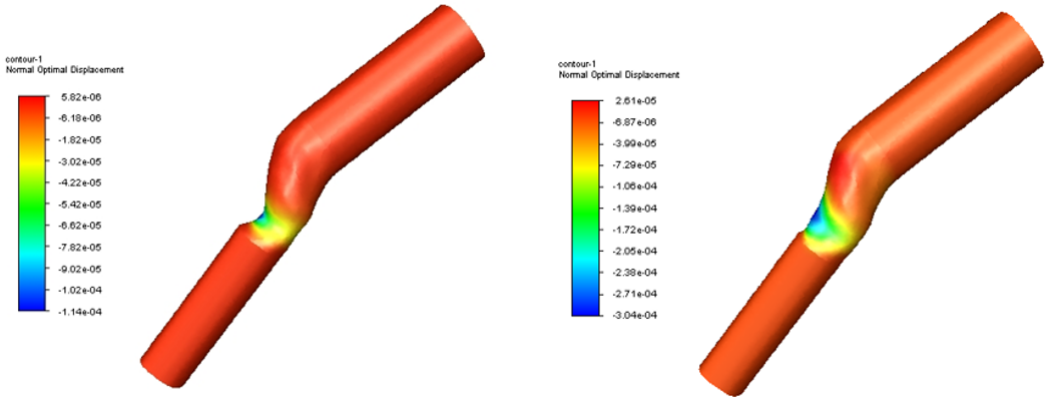

Figure 3.8: Normal optimal displacement for surface nodes of Case C, for early (left) and late (right) steps in the adjoint optimization. Positive values (red) indicate the optimal node displacement is inward; negative values (yellow to blue) indicate the optimal node displacement is outward.

as a B-spline [46] whose end points coincide with the native aorta centerline at the inlet and outlet faces. Tangency to the centerline is enforced at both ends of the graft centerline.

$$\vec{x} = \begin{bmatrix} x_1 \\ x_2 \\ x_3 \\ x_4 \end{bmatrix} = \begin{bmatrix} w_{inlet} \\ w_{outlet} \\ \gamma_p \\ d_p \end{bmatrix} \tag{3.5}$$

where w_{inlet} is the tangent weight at the inlet end of S_g and w_{outlet} is the tangent weight at the outlet end of S_g. A circular profile is constructed on a plane normal to S_g, with its centerpoint c_p coincident with S_g. We vary the location of c_p with the design variable $\gamma_p = ||\vec{c}_p - \vec{c}_{inlet}||$. Our fourth design variable is the diameter of the profile d_p.

Note that the number of variables required to define a graft shape increases

substantially with the size and complexity of the segment the graft replaces as in Figure 3.9. This example of transverse arch hypoplasia (TAH) would be best addressed by adding a patch graft to the underside of the aorta to increase the diameter along the arch without interfering with the brachiocephalic, left common carotid, or left subclavian arteries. The cost and difficulty of optimization increase as the number of design variables increases.

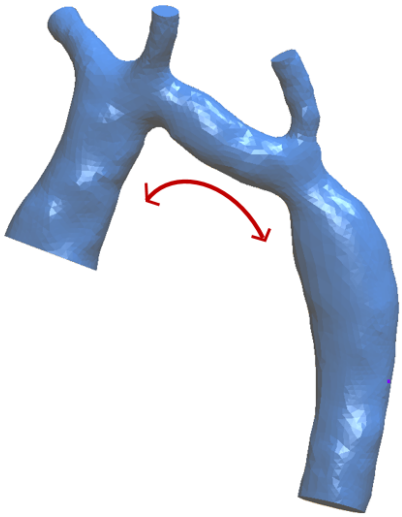

Figure 3.9: Aorta with transverse arch hypoplasia (TAH) that could require a patch graft to be inserted on the underside of the arch as indicated by the red arrow.

3.3.2 Building the Surrogate Model

Power loss as a function of graft geometry $P_{loss}(\vec{x})$ is not analytically known; to know the power loss for a graft represented by a point in the design space, we must simulate the hemodynamics. We therefore also have no knowledge of the gradient of the power loss with respect to the parameters of the graft design. As a result we cannot directly implement optimization methods that require gradients.

One way around this is to build a surrogate model $J(\vec{x})$ for the objective function that is easier to evaluate than the simulated graft performance. If the surrogate model is sufficiently representative of $P_{loss}(\vec{x})$, then a design $\vec{x}^*$ that minimizes $J(\vec{x})$ should also minimize $P_{loss}(\vec{x})$.

To build our $J(\vec{x})$, we sampled the design space from equation 3.5 and evaluated the objective at those points. We used the Latin Hypercube method [47] to select the sample points to efficiently cover the design space.

We fit a Gaussian process regressor (GPR) [48]to the sampled points $[X] = [\vec{x}_1, \ldots, \vec{x}_m]^T$ and their performances $\vec{y} = [P_{loss}(\vec{1}), \ldots, P_{loss}(\vec{m})]^T$. We used an RBF kernel with a length scale of 1.0.

To find $\vec{x}^*$ minimizing $J(\vec{x})$, we use an Upper Confidence Bound style algorithm where we successively sample points in J until our confidence level about the location of the minimum converges. In minimizing the surrogate, we fit the initial data points and then use an L-BFGS optimizer [49] to minimize the acquisition function. The acquisition function we use hedges between three acquisition functions at each point-selection iteration. Each of the three acquisition functions (lower confidence bound, negative expected improvement, or negative probability of improvement) is minimized for the current data set and the best candidate point of the three is selected. We weight the three criteria evenly in the selection of the best candidate point.

3.3.3 Surrogate Model Results: Case A

We tested the surrogate model on patient case A. We compare the optimal graft geometry suggested by the surrogate model to the optimal graft geometry suggested by the adjoint method described above. For patient case A, we found that our adjoint method designed a graft that achieved a 42% improvement over the native geometry in terms of power loss. The surrogate method described here achieved a 35.1% improvement over the same native geometry.

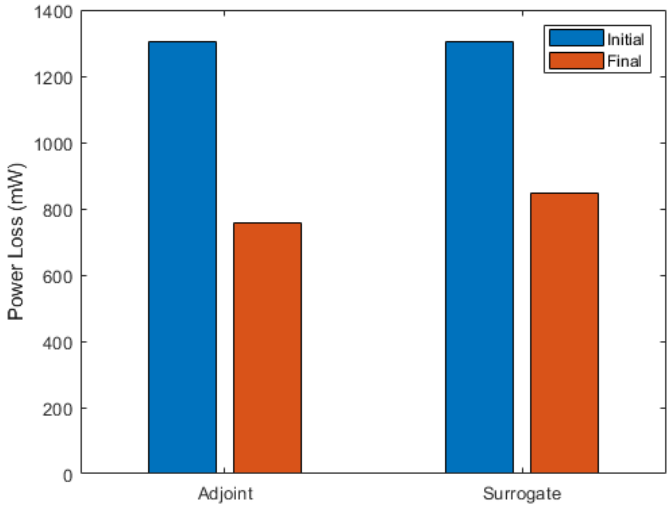

Figure 3.10: Power loss improvement over native geometry for Case A using adjoint and surrogate methods.

While additional tests on the other four cases would be advisable before drawing strong conclusions about the efficacy of the surrogate method, we note that the adjoint method slightly outperforms the surrogate method in terms of optimization of the objective function.

22 adjoint steps were required to achieve convergence for the adjoint method

when optimizing Case A, for a total of 44 simulations when considering that each step requires one forward and one adjoint CFD solution. The surrogate method presented here used a total of 11 forward simulations to achieve a similar improvement in the objective function.

While for this example we see similar performance for the surrogate model with a quarter of the simulations, we expect that as the complexity of the graft increases, the surrogate model would require substantially more design samplings.

3.4 Discussion and Summary

The optimizations performed in this thesis do not consider in detail the constraints imposed by the existence of other tissue and organs near the aorta. It is possible, though time-consuming, to extract the geometry of these constraining body parts from MRI data. An example of the data available can be seen in Figure 3.11. If extracted for a patient case, it is then trivial in concept to add no-go zones either by using the tools in the ANSYS Fluent Adjoint Optimizer [43], or by directly constraining mesh nodes that approach a boundary if using an external method for mesh node movements.

The automatic optimization method shown here produces patient-specific designs which substantially lower the power loss through the graft section when compared to the native tissue. The method does not guarantee optimality and may converge to a local minimum. However, the method does guarantee a topologically sound graft shape (i.e., the graft is water-tight). Further, it can be practically

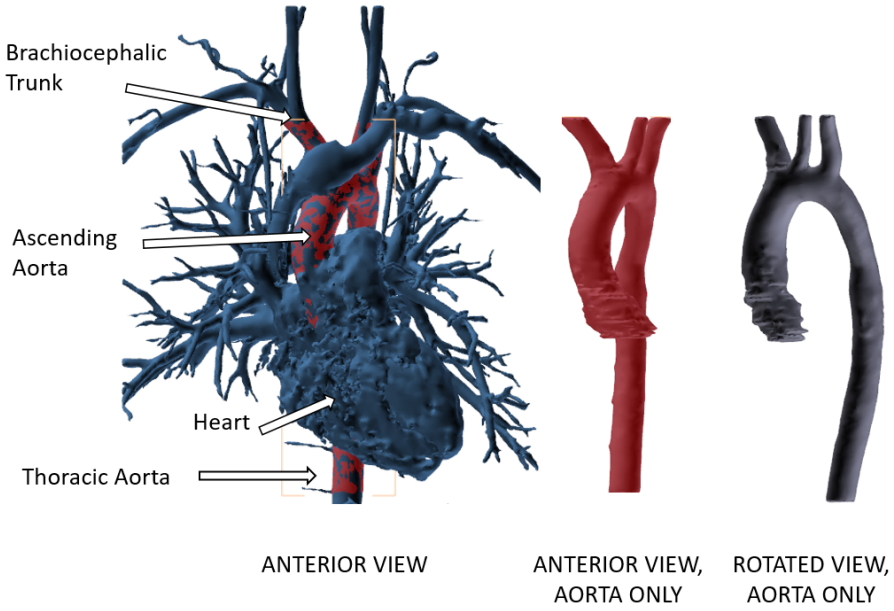

Figure 3.11: Geometry constraints (no-go-zones) imposed by the heart and vasculature.

implemented clinically on widely available computing hardware with an expected design turnaround time of roughly one day. Our optimized grafts show comparable performance to our models of traditional interposition grafts for these simple cases.

Using a method that uses adjoints at the mesh nodes allows for an extremely broad application of the method. As long as the forward and adjoint simulations converge, the method can be applied to any aorta geometry, even those with highly irregular shapes that may be difficult to represent using a parameterization. Our method does not require a parameterization, nor does it require consistently placed boundaries between native tissue to keep and native tissue to remove. Note that despite the large number of design variables (i.e. mesh nodes) and the iterative nature of the procedure, the results of the optimization are deterministic, as long as the same solver and CFD model settings are used. There is no stochasticity involved

in the mesh perturbation, i.e. selection of the next set of design variables.

Other optimization methods such as building a surrogate model require the developer of the method to make assumptions regarding the end points and dimensions along which the geometry varies. Particularly when extending the method to more complex cases in the future, building the surrogate model might only cover a subset of possible designs and be more expensive to compute than the automatic method using adjoints described here. Our method requires $2n$ low-fidelity simulations to converge, where n is the number of adjoint optimization steps – usually between 20 and 35. The full optimization takes on the order of 2 hours. A surrogate model in more than six dimensions likely requires at least 64 simulations in order to achieve a linear relationship between performance and each design variable. As a result, unless the simulations used to form the surrogate model are similarly low-fidelity and the number of design variables is quite low, our method likely requires fewer simulations and therefore less computational time.

Future work could include a more sophisticated approach to using the gradient information computed by the ANSYS Fluent Adjoint solver, for instance determining how best to apply a shape deformation algorithm. For these cases the graft endpoints were defined as simple perpendicular cuts chosen by an engineer, but the geometry preparation tools built on VMTK can be extended to allow a surgeon to define graft boundaries of more complex shapes. Another more difficult step to achieve is that the lower-fidelity simulations required for the adjoint solution must be be made to converge for the more complex shapes. While the ANSYS solver has a number of limitations that make this impractical, the method of iteratively opti-

mizing using sensitivities can be achieved using a variety of solvers and geometry strategies, making this a promising direction for future work.

Chapter 4: Main Experiments: Impact of boundary conditions

While the previous chapter presented a method for optimizing a patient-specific graft, this procedure depends on some unknown inputs such as the patient's arterial flow velocity and pressure. How robust is that optimal graft design, given that we may only have approximate (uncertain) measurements of those boundary conditions? This chapter addresses this question by studying how much optimal grafts deviate when we alter the specific flow values within clinically relevant ranges. It compares these optimized grafts in both performance (changes in power loss) and geometry (changes in the graft mesh measures via Hausdorff distance [50]).

Some work has been done in the past to examine the sensitivity of CFD models for arterial flow with respect to model parameters. A study was done for coronary artery bypass grafts of the sensitivity of estimated shear rate near the artery wall with respect to fluid viscosity [51]. Another study examined the sensitivity of pressure drop predictions with respect to the applied volume flows in the interest of predicting pressure drop instead of making invasive measurements [52]. Neither of these studies evaluated the sensitivity of optimal geometry predictions with respect to model parameters. This chapter explores that question.

4.1 Methodology

4.1.1 Metrics

We evaluate the performance of the grafts by calculating the improvement in power loss of the optimized graft compared to the power loss of the initial native geometry.

To calculate differences between two possible graft geometries, we use the root mean square of the one-directional Hausdorff distance [50]. Specifically, we compute the distance between two grafts A and B by sampling points on the graft A's surface and finding the shortest distance to a node on the surface of graft B. For n sampling points p taken from graft A, the distance between grafts A and B is

$$\text{Distance}(A, B) = \sqrt{\frac{1}{n} \sum_{p \in A_p} \left(\min_{p' \in B} (p - p') \right)^2} \tag{4.1}$$

The set of sampling points for all distance measurements made in this chapter is the set of all mesh nodes in graft A (excluding those in the flow extensions). In all comparisons, graft A is taken to be the patient case's optimized design for $v_{in} = 0.5 v_{peak}$. The distance metrics were computed using MeshLab [50], facilitated by the MeshLabXML Python scripting interface [1].

This method does not assume any correspondence between the mesh topology of the geometries being compared. That is, even if remeshing is necessary in the course of the optimization, or if a different initial mesh is used, the similarity

[1] https://github.com/3DLIRIOUS/MeshLabXML

measurements can still be computed.

4.2 Experiment 1: Velocity Magnitude

To evaluate how the optimized grafts (Chapter 3) change in response to differing boundary conditions, we optimized a graft design for each patient case for velocity input conditions ranging from 20% to 120% of peak systolic velocity. We chose this range of velocities since it represents a wide but clinically relevant bound on patient uncertainty. In practice, current medical imaging can achieve more precise bounds on the peak systolic velocity. This means that our below results are a conservative estimate.

During optimization, we targeted a 5% improvement in pressure drop at each adjoint step. The optimizations typically take 25-35 adjoint steps with a total wall-clock time of roughly one hour on a desktop workstation. We evaluated graft similarity in two ways. First, via performance similarity—or how similar the hemodynamic flows are across each graft. This similarity helps quantify the robustness of patient outcomes. Second, via geometric similarity—or how similar the actual geometric meshes of the grafts are. This similarity helps us understand how sensitive the final electro-spun TEVG is to uncertainties in the imaging data.

4.2.1 Performance Similarity

Power loss through a graft depends on the velocity of the fluid moving through the graft. In this experiment, we have generated several grafts for each patient case

– each designed using a different velocity condition. To appropriately compare the graft designs generated at different velocities, we need to subject each graft to the same conditions and compare those performances. For instance, we would like to compare the graft optimized with $V_{in} = 0.3 \cdot V_{peak}$ to the graft optimized with $V_{in} = 0.7 \cdot V_{peak}$. A fair comparison would be to simulate both final graft geometries using identical conditions.

Therefore, to evaluate the similarity of hemodynamic performance, we ran a set of forward CFD simulations to predict the power loss through the grafts designed at 30, 40, 50, 60, and 70% of the peak inlet velocity. Each graft's power loss was modeled at all five of the design velocities. The method for each patient case is as follows:

1. For each velocity:
    (a) Let this velocity be considered the "design velocity"
    (b) Apply the design velocity as the inlet boundary condition and use the adjoint optimization method to generate an optimized graft, starting with the patient's native geometry.
    (c) Calculate the power loss when this optimized graft is subjected to the design velocity.
    (d) For each velocity not used to optimized this graft:
        - Let this velocity be considered the "validation velocity".
        - Run a forward CFD simulation using this optimized graft and applying the validation velocity as the inlet boundary condition.

- Calculate the power loss when this optimized graft is subjected to the validation velocity.

4.2.2 Results

Below we compare the effect of the varying boundary conditions along the following criteria: (1) graft power loss performance, (2) differences in geometry, (3) effects of varying inlet pressure, and (4) the impact of varying flow extension shape.

4.2.2.1 Performance Comparison

To understand the effects of these geometry differences on graft performance (power loss), we simulated all five designs at all five inlet velocities. Figure 4.1 shows the power loss for each graft designed for case A at each velocity. We found that grafts designed using velocities within 20% of nominal velocity have predicted power loss within 2.5% of the predicted power loss for the grafts designed at nominal velocity.

4.2.3 Geometry Comparison

We found that for velocities within 20% of the nominal value, the Hausdorff distance metrics indicate that there is little difference between the optimized geometries (see Figure 4.2). For cases A and C, the maximum nodal Hausdorff distance between optimized meshes is less than 0.3 mm, or less than 5% of the final diameter at the former site of the coarctation. The maximal nodal Hausdorff distances fluc-

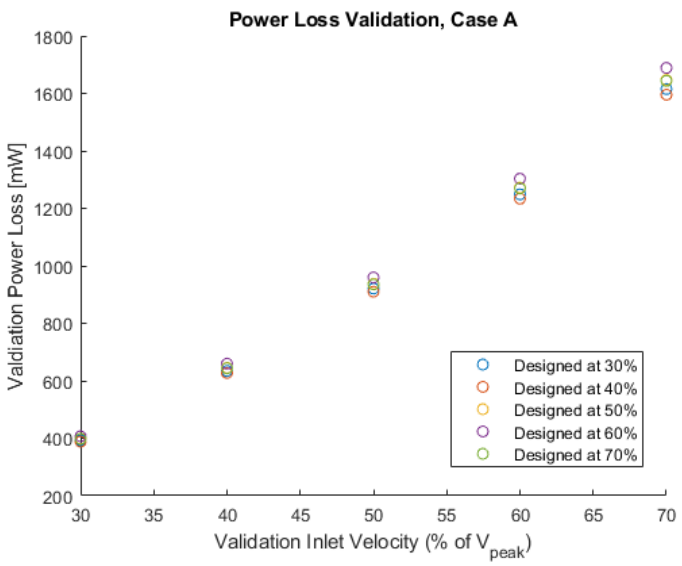

Figure 4.1: Power loss predicted by applying each inlet velocity to each optimized graft design for Case A.

tuate quite a bit for case B, though the RMS distances are quite low, indicating that the impact of initial geometry configuration may be more important than velocity conditions.

Note that Case D has the most extreme initial geometry as shown in Figure 3.2. The difficulty of addressing the large mesh shifts required in the stenosed area without completely remeshing is likely the cause of the discrepancy.

4.2.3.1 Pressure

One benefit of the method we describe here is that due to the assumptions made in setting up the CFD model, pressure conditions have no impact on the resulting graft. We apply a pressure condition on the outlet, but no pressure condition on the inlet. Setting the outlet pressure to 0Pa in every case is a valid choice for our method. We verified the results by running the optimization with

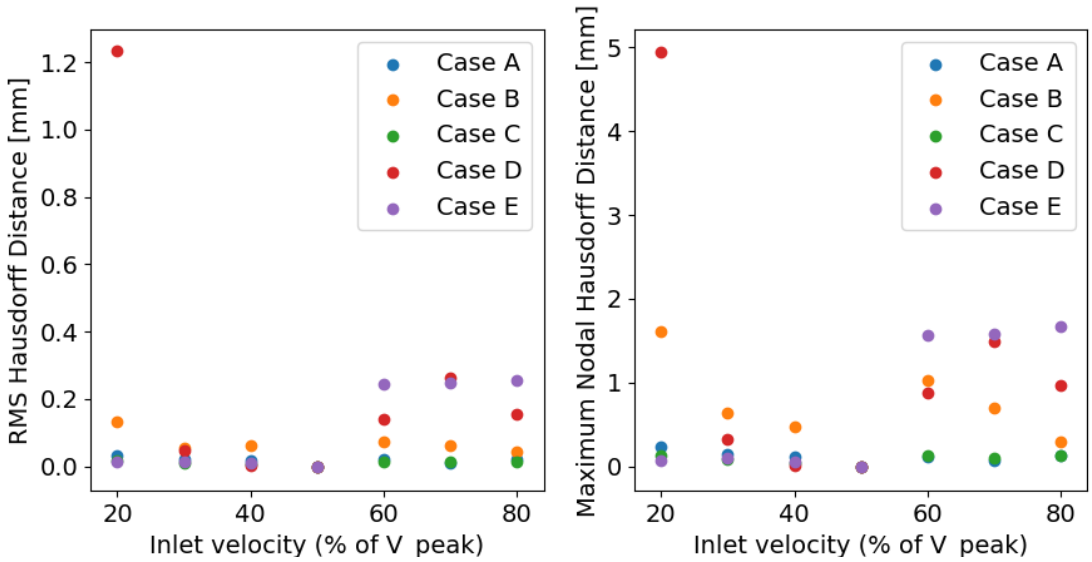

Figure 4.2: Distance metrics comparing graft geometries optimized using different velocities.

$P_{outlet} = \{0Pa, 0.5 \cdot \Delta P_{systolic}, \Delta P_{systolic}\}$. As shown in Figure 4.3, the model is unaffected by the choice of outlet pressure. Further, Table 4.1 shows that the nodal positions of the final grafts were identical for each pressure. That is, for a given patient case, the outlet pressure boundary condition has no impact on the final graft shape.

Case	Max, P_{med}	Max, P_{high}
Case A	0.0	0.0
Case B	0.0	0.0
Case C	0.0	0.0

Table 4.1: Hausdorff distance calculations for pressure study

4.2.3.2 Flow Extensions

To assess the impact of another aspect of patient-specific flow on the grafts recommended by our method, we generated new models for each patient case to

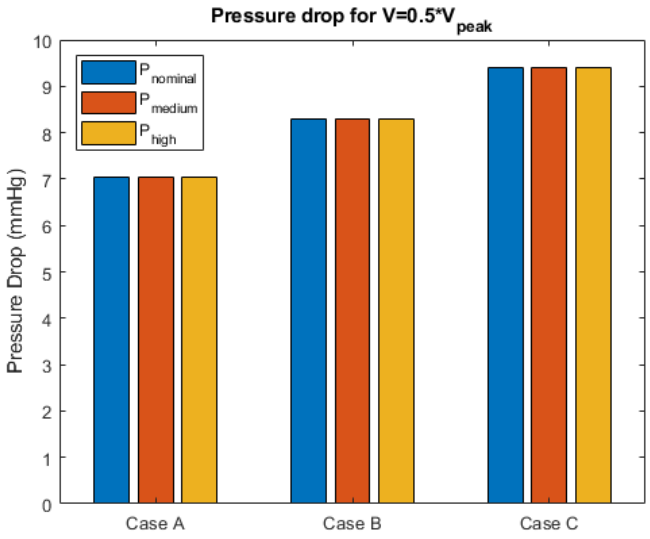

Figure 4.3: Pressure drop at final adjoint step for nominal, medium, and high outlet pressure boundary condition.

induce more physiologically-accurate flow profiles at the true inlet of the graft segments. The profile of the graft inlet was swept along the centerline extracted from the aortic arch (see Figure 4.4) for a path length equal to the length of the straight extensions used in the pilot study as described in Chapter 3.

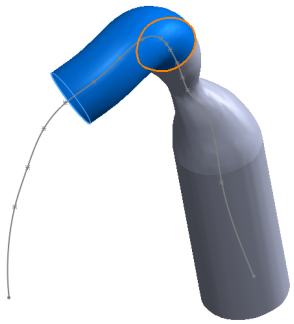

Figure 4.4: Construction of the curved inlet extension for patient Case D. The inlet profile (orange) is swept along the centerline to produce the patient-specific curved inlet extension (blue).

The five new initial patient case geometries are seen in Figure 4.5.

As in the pilot study, a constant velocity is applied to the inlet of the extension.

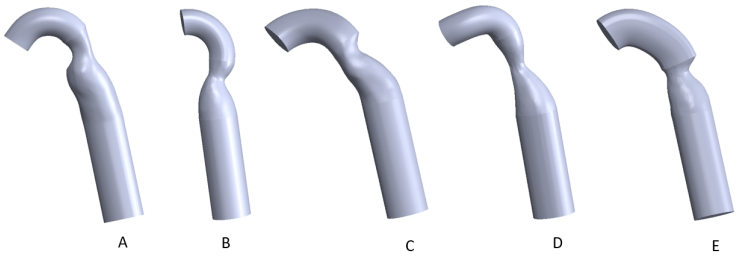

Figure 4.5: Coarctation geometries prepared for curved extension study.

Non-slip conditions are applied to the extension and graft walls. As a result, the cross-sectional velocity profile at the true inlet of the graft itself fully develops to have a somewhat parabolic character. The curvature of the inlet creates a perturbed less-symmetrical flow front as seen in Figure 4.6.

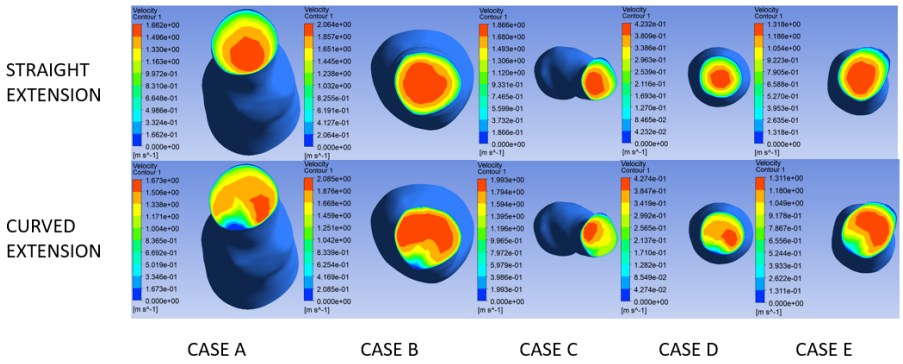

Figure 4.6: Velocity profiles at true graft inlet for straight and curved inlet extensions.

To compare the grafts generated by straight and curved inlet extensions, we employ the algorithm as described in Chapter 3. We apply 50% of the peak systolic velocity from Table 3.1 to the inlet of the new models with curved extensions. We seek to quantify the impact of applying a velocity condition that reflects the curved nature of the aorta on the geometry and performance of the graft recommended by our method. We make the comparison on the basis of percentage improvement

in pressure drop and on the basis of Hausdorff distance between the two grafts suggested for a patient.

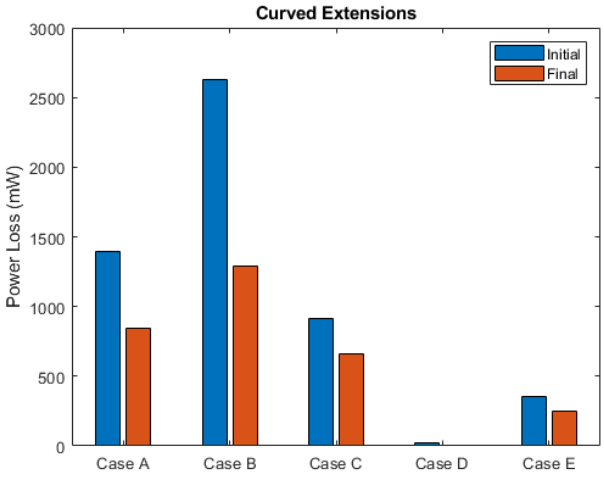

Figure 4.7: Power loss performance for initial and final grafts using curved inlet extensions.

We found that the method using curved extensions, like the method using straight extensions, was able to generate better than 25% improvement in power loss. We find that curved extensions do not generally improve the power loss performance of the suggested optimal patient-specific grafts.

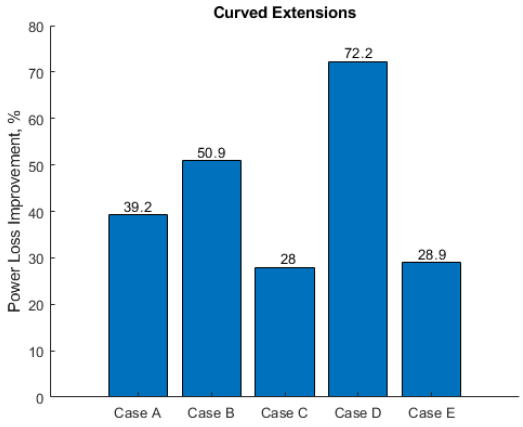

Figure 4.8: Percentage improvement in objective from initial to final graft generated with curved inlet extension

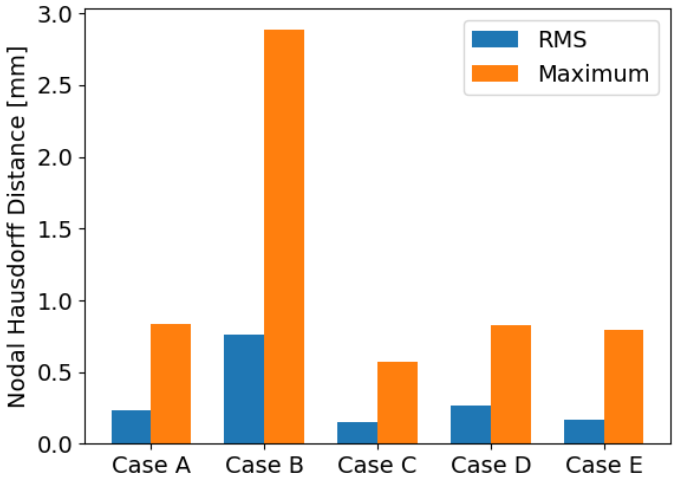

Figure 4.9: Hausdorff distance metrics calculated for straight-vs-curved extension graft designs.

Note that case D is once again a slight outlier, in that its percentage improvement in the objective using curved extensions is worse rather than better or comparable, unlike the other four cases as shown in Figure 4.10. We see also that case D with curved extensions has by far the largest Hausdorff distance between its native and optimized geometries. This, again, we attribute to the extremity of the initial stenosis and the associated mesh update issues. Future work could implement strategies for a more comprehensive mesh quality check and update, or as discussed in Chapter 5, a clever initial geometry could be used rather than the native geometry.

4.3 Summary

Chapter 2 optimized a graft for a specific patient under a single velocity input condition. In this chapter we showed that such optimal grafts are insensitive to

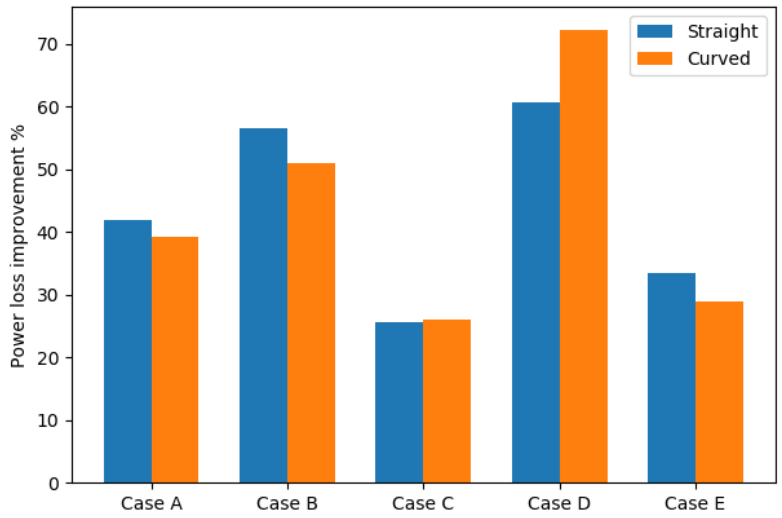

Figure 4.10: Percentage improvement in power loss compared for straight vs. curved inlet extensions.

the choice of input velocity. Our results show that for the purposes of graft design optimization, applied inlet velocity need only be within 20% of one half of the peak systolic velocity in the descending aorta in order to generate a mesh that deviates by no more than 5% of the average diameter of the graft. For all applied inlet velocities, predicted power loss fell within 2.5% of the power loss predicted for the graft designed with nominal inlet velocity. This has clinical importance because this reduces the need to have precise flow measurements for an individual patient, alleviating some imaging concerns.

Chapter 5: Preliminary Results: Learning to Warm Start Graft Optimization

While Chapter 2 described how to use adjoint-based optimization to modify the initial coarctation into an optimal graft, the algorithm spends many of those optimization steps near the known poor geometry of the original coarctation. But what if we could start the optimizer closer to a good final geometry and then just optimize from there? This idea—sometimes called "warm starting" an optimization process—tries to pick a good initial guess such that we limit the number of optimization steps (and time) required or to improve the optimizer's stability. In practical terms, this could mean designing an optimal graft for a patient in a handful of hours rather than an entire day (as in Chapter 2).

To get a feel for the impact of a 'good' initial geometry, we design an initial shape for Case B using a simple loft constrained to be normal to the inlet and outlet profiles. The lofted initial geometry is compared to the native initial geometry in Figure 5.1. Intuitively, the lofted shape should have lower power loss as there is no stenosis.

We then run our adjoint optimizer on each initial geometry, using otherwise identical boundary condition and convergence values. We find that the graft opti-

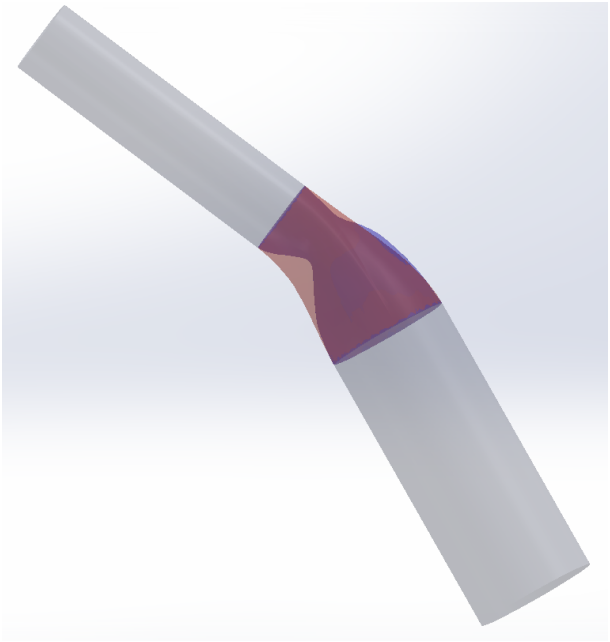

Figure 5.1: Overlay of native (blue) and lofted (red) initial geometries for Case B.

Step	P_{loss}	Percent Improvement
1	1.1093	0.00
2	1.1017	0.68
3	1.0970	1.10
4	1.0939	1.39
5	1.0971	1.10

Table 5.1: Power loss at each adjoint optimization step for Case B optimized at nominal velocity using the lofted initial geometry.

mized using the native geometry as a starting point achieves a power loss of 1.12 W, which is higher than the initial lofted configuration which achieved a power loss of 1.093.

The graft optimized using the lofted geometry as a starting point only has 1.39% lower power loss than the initial loft itself.

These sorts of coarctations in the descending aorta are geometrically simple, so it is unsurprising that the lofted solution achieves a very good power loss performance by smoothly interpolating between the inlet and outlet. Extending this

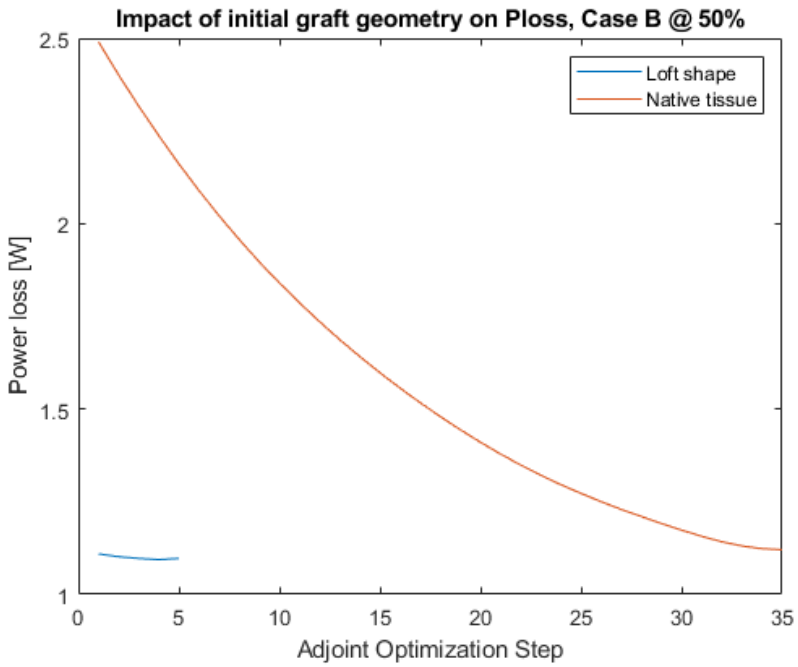

Figure 5.2: Graft performance at adjoint iteration steps starting with the native tissue or a lofted guess. Note that beginning with a lofted shape requires only 5 adjoint steps to reach the optimal geometry.

idea to a patch or branching graft becomes more complicated. Therefore we want to investigate a method of producing good initial guesses.

One method for producing these good initial guesses to warm start the optimizer is via machine learning. This approach often uses the term "inverse design" to refer to a process of trying to invert the optimal geometry given some input conditions. In principle, we think it would be possible to build a useful machine learning model that can predict the optimal 3D graft geometry given the patient inlet and outlet locations and some velocity conditions from the pre-repair MRI. In practice, however, the size of the patient datasets available to us is extremely small (on the order of n=10) and expensive to collect, relative to the amount of data required to build a useful machine learning model.

Despite lacking a large dataset of segmented MRIs, an alternative approach to building an inverse design dataset is to generate our own optimal geometries via simulation. This chapter demonstrates this concept on branched geometry with a single inlet and two outlets in two dimensions.

Specifically, we establish a set of values that define our constraints on the system such as the location of the inlet, the location of the two outlets, and the inlet velocity. We also set a parameter on the fraction of the domain that can be 'inside' the pipe—that is, we fix the volume fraction of material in our topology optimization. We then use the FEniCS Dolfin adjoint optimizer for computational fluid dynamics (CFD) to optimize the geometry for power loss, assuming Stokes flow. While future work could explore advanced optimization and flow simulation methods, this chapter uses these simpler and faster-to-run models to demonstrate the overall concept.

5.1 Methodology

5.1.1 Dataset Generation

Each point in our data set is an output of a converged topology optimization run via the FEniCS and dolfin-adjoint simulation library. The mesh used to generate this data set is a 51x51 square domain, where $x_{in} \in [0, 1.0]$ and $y_{in} \in [0, 1.0]$. Each simulation targets a geometry that takes up 40% of the domain (*i.e.*, has a 40% volume fraction).

We have the coordinates of each mesh point and three fields defined on that

mesh: density, velocity, and pressure. For the purposes of this model we disregard the velocity and pressure fields except to note the velocity vectors applied across the inlet. While a normal distribution with some noise was used to set up the velocity inlet in simulation, for the purposes of our model we will keep only the midpoint coordinates of the inlet and the average velocity vector.

Our input vectors contain the x and y coordinates of the center of the inlet, the x and y components of the average inlet velocity, the magnitude of the inlet velocity, the x and y coordinates of outlet 1, and the x and y coordinates of outlet 2.

$$X[i] = [x_{in}, y_{in}, v_{x,in}, v_{y,in}, ||v||, x_{out,1}, y_{out,1}, x_{out,2}, y_{out,2}]$$

The output that we are trying to predict is the density field—this field represents the optimal pipe geometry for that set of input conditions. We can treat this as a classification problem by applying a threshold on the density and considering any cell whose value is higher than that threshold to be inside the pipe and all other cells to be outside the pipe.

Our output vectors $y[i]$ are 1 by 51^2 dimensional arrays where each entry is either zero or one as described above.

5.1.2 Learning approach

The prediction of pipe geometry in the format we are using is a supervised classification problem. The model must predict, for each cell in the mesh given the input vector x, whether it is inside or outside of the pipe. We chose to implement

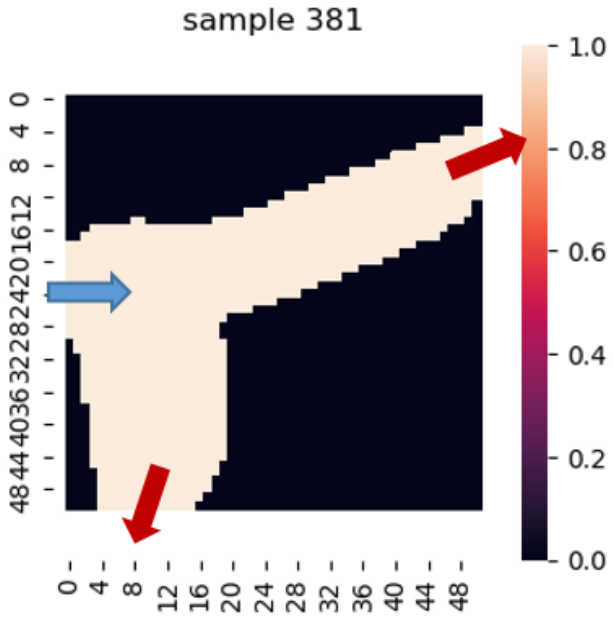

Figure 5.3: Output data point $y[381]$ with inlet and two outlets indicated.

two types of classification: K nearest neighbors (KNN) and Kernel Ridge Regression (KRR). We chose these specific models since they are (1) fast, (2) non-linear, (3) well-understood, (4) possess few hyperparameters, and (5) can provide a competitive baseline for future efforts in this area [53].

K Nearest Neighbors The K nearest neighbors model finds the k closest neighbors in the input space and interpolates their output values. That is, KNN predicts that the value of a cell will be the average of the cell values of the k nearest neighbors. We used k=5 for all KNN models shown below.

Kernel Ridge Regression Kernel ridge regression combines the kernel trick (in this case we use a Radial Basis function for the kernel) with a ridge regression penalty.

In addition to classifying the geometry on the original output data, we also

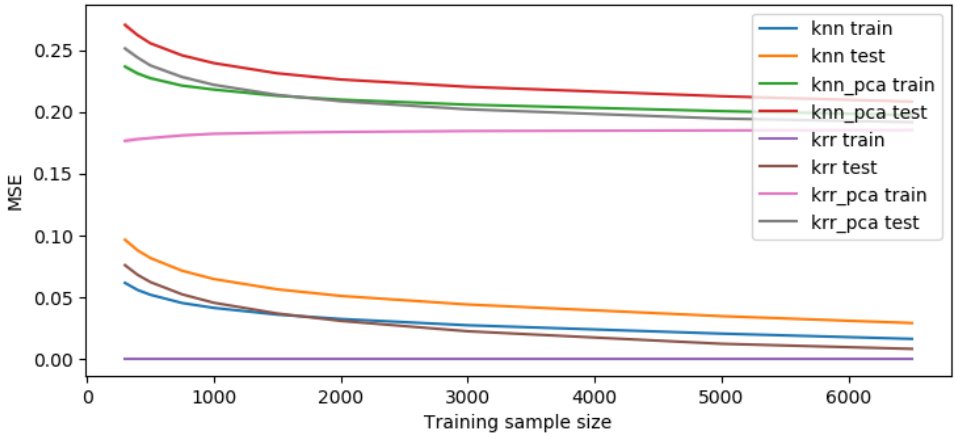

Figure 5.4: Mean square error of models implemented. Note that the error inherent in reconstructing the y vectors from the primary components mean that this is not a viable strategy for small 2D meshes.

hypothesized that the true classification surface would be low-dimensional (in the space of mesh coordinates). As such, we anticipated that we might achieve better results by projecting the original input space onto a lower-dimensional space spanned by the coefficients of their first 300 primary components via Principal Component Analysis [54]. We then trained KNN and KRR using those output vectors and compared the accuracy of those results to those same models without the dimension reduction strategy.

5.2 Results

We tested the above models using a shuffle split cross validation [55] with 15 splits on a data-set size of 9000 generated optimal geometries. We calculate the Mean Squared Error on the test-set for each model and Figure 5.4 plots these test MSEs as a function of the amount of training data used.

We found that PCA caused the MSE to increase substantially due to the loss of

resolution when reconstructing the output vectors. Contrary to our original hypothesis, the reduced dimensional space did not provide a corresponding benefit in the sample efficiency compared to the basic KNN and KRR models. KRR outperformed KNN at all training set sizes.

5.3 Discussion

One caveat to this specific analysis is that the data set we generated contains samples with inlet/outlet configurations that are unlikely to be encountered in the intended application—surgical repair of aortic coarctations. For example, inlet and outlet conditions with sharp turns in the domain due to how we randomly placed the inlet and outlet locations along the boundary when generating the dataset. Such data points likely add a bias toward more material near the inlet as seen in Figure 5.5. This bias in our dataset generation means that the prediction task for aorta-like geometries is likely to be easier and more accurate than the results in Figure 5.4 suggest.

5.4 Summary

For this data set, a simple KRR model performed the best and was able to predict optimal geometries with an MSE below 0.05. We expect that when the dimension of the mesh increases, PCA could become a more useful tool, however we did not observe any benefit to using PCA as a pre-processing step in this chapter.

Future extensions of this work can include the generation of a CFD test data set

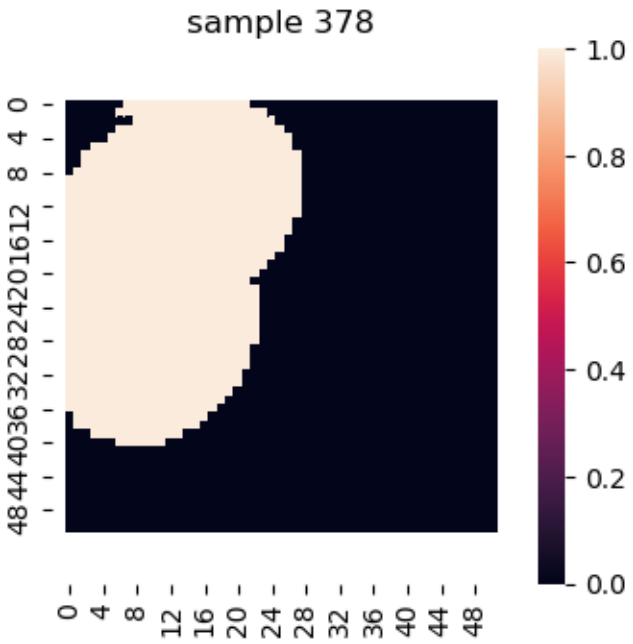

Figure 5.5: An example of an unrealistic inlet/outlet configuration that was not excluded from the analysis.

that uses fluid dynamics conditions more closely resembling those seen in the aorta, as well as extending the model to 3D geometries. We expect under these additions the prediction task will become more difficult and require additional training data to achieve similar accuracy. In contrast, the more well-behaved nature of aorta geometries will also likely make the problem slightly easier and improve the sample efficiency compared to random boundary locations.

Chapter 6: Conclusion

The goal of this thesis was to investigate automatic methods for designing hemodynamically optimized patient-specific tissue-engineered vascular grafts (TEVGs) for aortic arch repair. Solving that problem has wide ranging clinical impact because this procedure addresses congenital heart disease (CHD), which causes roughly 4,000 deaths annually in the United States, more than any other type of congenital anomaly [1, 2].

Specifically, in Chapter 3, we developed an automatic design method for TEVGs for repairs of the descending aorta via an adjoint solver. We found that the proposed approach takes around 20-35 steps to converge on aortic coarctations, which had a compute time of 2 hours total on a desktop workstation. Compared to a baseline model using a Gaussian Process Surrogate Model, we expect that the proposed model will be more efficient than the baseline if the design representation for the Gaussian Process exceeds six dimensions, and less efficient if the surrogate model uses less than six dimensions. In the simple coarctations considered in this thesis, surrogate model approaches are likely comparable and easier to use, however, in more complex aortic arch repairs, such as patch repairs, this should not be the case.

In Chapter 4, we investigated the robustness of the found repair geometry with respect to inlet velocity, which is often uncertain and estimated using flow measurements. We found that, for the purposes of graft design optimization, the applied inlet velocity needs to be estimated to only within 20% of one half of the peak systolic velocity to generate optimized geometries that deviate by no more than 5% and deviate in power loss by no more than 2.5%. More, that chapter showed that patient inlet pressure conditions or measurement uncertainty did not affect the resulting optimal geometry. This is clinically important because gathering patient-specific pressure conditions requires either invasive catheter placement, which introduces complication risks, or estimating pressures via cuff pressure measurements, which introduces significant error. Given that the pressure condition has limited effect on the final optimized geometry, this significantly relaxes the patient risk and cost needed to determine the appropriate graft geometry. Lastly, that chapter studied the effect of model simplifications—via flow extensions needed to develop flow fronts for resolving the adjoint calculations—on the final optimized geometry. It shows that using the appropriate extension shape (specifically a curved shape) can better match the flow profile of the patient compared to straight extensions, while still allowing the solver to compute the adjoints needed for the gradient based optimizer.

In Chapter 5, we briefly investigated the robustness of the method with respect to the initial geometry and study the usefulness warm-starting the optimizer with a machine-learning approach. We found that, for the simple coarctations discussed in this thesis, a simple, deterministic lofted tube around the defined cut points of

the graft does exceptionally well, producing repair geometries that are within 1.39% of the final optimized power loss, and reduced the number of required adjoint steps from between 20-35 to between 3-5 until convergence. To attempt to improve upon this, we propose a machine-learning approach to infer the optimal geometry directly (i.e., conduct inverse design). We demonstrate this in 2D where the best models where able to predict topologically optimized branched flow channels to within 0.05 Mean Squared Error on the density field. While the machine learning approach is not as useful as the deterministic lofted-tube case for the simple coarctations considered in this thesis, we expect that such strategies may be more useful for more topologically complex repairs such as those involving branched geometry in the head of the aorta. In such cases, simple lofted surfaces will likely not suffice for capturing close-to-optimal warm start geometries, though future work would need to address that specific hypothesis.

This main contributions of this thesis are:

1. Investigating automatic optimization of patient-specific tissue engineered vascular grafts via adjoint methods, which produces graft designs that improve the power loss of native stenosed tissue by 25-60%. While it demonstrates this for simple coarctations in the descending aorta, it extends to more complicated graft shape applications in the head of the aorta where competing techniques, such as Surrogate models, would suffer from the curse of dimensionality.

2. Quantifying the robustness of optimized graft geometry with respect to key clinical measurements, such as the velocity and pressure flow conditions. We

find that similar grafts are generated provided the flow velocity used to design the graft is within 20% of the nominal velocity, and that pressure changes have negligible effect. This has important implications for the accuracy of clinical flow measurements, such as not requiring invasive pressure measurements or highly accurate flow data derived from MRI, which sheds light on the kind of clinical requirements and measurements need for design optimization to provide value.

3. Evaluating the impact of the type of velocity profile applied at the true inlet of the graft by adjusting the shape of the extension applied at the inlet during geometry pre-processing.

4. Studying the benefits to various warm-starting strategies for the optimization including both deterministic lofted profiles for simple tube repairs as well as machine-learned estimators for branched geometry. We show that significant gains can be made in optimization time and effort (up to an order of magnitude time reduction) by appropriate warm-starting.

6.1 Limitations

6.1.1 Extension to Branching Geometries

The cases considered in this thesis consist only of simple coarctations distal to the left subclavian artery. As a result, the natural geometric simplification of the CFD model involves preparing a mesh only of the descending aorta. Then the

hemodynamics we model in this portion of the aorta can be as accurate as our knowledge and application of flow conditions at the inlet of this area of interest.

Our method described in Chapter 3 could very well be implemented for cases where branched grafts are required, provided the CFD model is compatible with the adjoint solver in use. Two changes to the method would be required. First, the pressure boundary conditions must be determined (possibly through cuff pressures measured on the upper and lower extremities). Second, we can and perhaps ought to encourage a particular flow split by modifying our objective function to be a linear combination of the existing objective (power loss) and a term measuring the 'error' between the difference in mass flow to the two outlets and our desired difference.

One area of uncertainty that we cannot address with the single-inlet, single-outlet model is the degree to which changes to the descending aorta geometry will impact the flow splits to the various arteries (see Figure 1.2). Validation of the output optimized graft using a full-aorta simulation could evaluate the impact of this uncertainty.

6.1.2 Optimality of Adjoint Solutions

In order to prove that a graft designed by our method is a global optima, we would need to prove that the graft design is a local optima and further that the problem is convex (that is, that the objective function is convex and any constraints meet the constraint qualifications). Showing that a design is a local optima requires knowledge about the gradient and Hessian at that point: the gradient must

be zero, and the Hessian must be positive semidefinite. Showing that a local optima is in fact a global optima requires the additional step of showing that the problem is convex [56]. It is clear then that showing that a given design is a local or global optimum is difficult if not impossible for the problem considered in this thesis: optimizing a high-dimensional non-differentiable objective using relatively time-intensive evaluations. Future work could focus on building a surrogate model of the the CFD objective as in Quarteroni and Rozza [32].

Further difficulties in determining the true optimality of the solutions we describe arise from the nature of adjoint problems. Some strategies exist to deal with solving adjoint problems when convexity cannot be proven [57], but are beyond the scope of this work.

In this work we therefore chose to focus on practical indications that our method repeatably give the same solution despite perturbations to the initial conditions such as velocity, pressure, and initial geometry (apart from the inlet/outlet locations, which we consider to be fixed). For instance we show in Chapter 5 a comparison of the results of our optimization method using two different initial graft geometries for the same patient case, finding that the resulting optimized graft is quite similar regardless of initial geometry. Future work could more thoroughly quantify the space of initial designs which results in the same optimized geometry.

6.1.3 Saddle Points

Without knowing anything about the convexity of this problem, we could have found what appears to be a minimum but is in reality a saddle point, where the gradient provided by the adjoint sensitivities reaches zero but a better design point could be obtained using a slight perturbation of the design in a direction orthogonal (in the design space) from the direction that the gradient approaches zero from above. Without a way to determine the definite-ness of the Hessian, we cannot state for sure that we have achieved a minima rather than a saddle point [56].

6.1.4 Adjoint Solver Limitations

As discussed above, the adjoint simulations used in this automatic method can be extended to cases with multiple outlets (i.e., branched grafts). However, there are some technical limitations imposed on the complexity of CFD model by certain adjoint solvers that may make this difficult. For instance, ANSYS Fluent 19.2 does not permit outflow-type (mass or volume flow at an outlet) boundary conditions to be imposed on models to be solved with the Adjoint solver. Further, transient models cannot be used. In theory, adjoint sensitivities can be computed for such models, though the computational time required for adjoint sensitivities of non-steady-state models using contemporary hardware can be disqualifying. As computational capabilities increase, these limitations could become unimportant.

6.1.5 Steady-state Pressure constraint simplification

The steady-state assumption made in the CFD model removes some of the complexity of the hemodynamics from the problem. As discussed in Chapter 2, several studies have investigated the difference in hemodynamics predicted by complex fluid-structure interaction (FSI) models, rigid walls with compressible fluid, rigid walls and incompressible fluid, and steady-state rigid walls with incompressible fluid and found that while certain measurements such as wall shear stress may differ in magnitude, a qualitative comparison of aortas can be made using simplified models [26, 44]. Future work could undertake a more thorough validation of the model using comparisons to transient full-aorta simulations.

6.2 Future Work

Future work could engage with several different parts of the optimization method. First, the definition of graft boundaries was limited to simple cuts perpendicular to the centerline of the descending aorta. The tool used to identify boundaries, VMTK, can be extended to allow irregularly-shaped patch boundaries to be identified anywhere on the aorta. Second, a more sophisticated method for the mesh morph could be used. The method currently has no understanding of the branching-tube structure of an aorta; mesh modifications maintain some smoothness, but are highly localized. Therefore, some knowledge about the typical smooth annular structure of a blood vessel could be applied without requiring a full parameterization of the aorta.

The investigation into warm-starting the optimization process from Chapter 5 has a number of possible extensions. A larger study of the impact of initial geometry shape could be undertaken. Additionally, with the generation of a 3D branched-pipe data set, we could begin to investigate a geometry decomposition that would allow for a learned parameterization of the geometry of different classes of aortic graft (i.e. different inlet/outlet topologies).

Bibliography

[1] Suzanne M. Gilboa, Jason L. Salemi, Wendy N. Nembhard, David E. Fixler, and Adolfo Correa. Mortality Resulting From Congenital Heart Disease Among Children and Adults in the United States, 1999 to 2006. *Circulation*, 122(22):2254–2263, November 2010.

[2] T. J. Mathews, Marian F. MacDorman, and Fay Menacker. Infant Mortality Statistics from the 2013 Period: Linked Birth/Infant Death Data Set. Technical report, American Psychological Association, 2015. type: dataset.

[3] Jan L. Bruse, Silvia Schievano, Maria A. Zuluaga, Abbas Khushnood, Kristin McLeod, Hopewell N. Ntsinjana, Tain-Yen Hsia, Maxime Sermesant, Xavier Pennec, and Andrew M. Taylor. Detecting Clinically Meaningful Shape Clusters in Medical Image Data: Metrics Analysis for Hierarchical Clustering Applied to Healthy and Pathological Aortic Arches. *IEEE Transactions on Biomedical Engineering*, 64(10):2373–2383, October 2017.

[4] Takuma Fukunishi, Cameron A. Best, Tadahisa Sugiura, Justin Opfermann, Chin Siang Ong, Toshiharu Shinoka, Christopher K. Breuer, Axel Krieger, Jed Johnson, and Narutoshi Hibino. Preclinical study of patient-specific cell-free nanofiber tissue-engineered vascular grafts using 3-dimensional printing in a sheep model. *The Journal of Thoracic and Cardiovascular Surgery*, 153(4):924–932, April 2017.

[5] Joong Yull Park, Chan Young Park, Chang Mo Hwang, Kyung Sun, and Byoung Goo Min. Pseudo-organ boundary conditions applied to a computational fluid dynamics model of the human aorta. *Computers in Biology and Medicine*, 37(8):1063–1072, August 2007.

[6] Hussam Suradi and Ziyad M. Hijazi. Current management of coarctation of the aorta. *Global Cardiology Science and Practice*, 2015(4):44, September 2015.

[7] Julien I.E Hoffman and Samuel Kaplan. The incidence of congenital heart disease. *Journal of the American College of Cardiology*, 39(12):1890–1900, June 2002.

[8] Rachel D Torok. Coarctation of the aorta: Management from infancy to adulthood. *World Journal of Cardiology*, 7(11):765–775, 2015.

[9] Maximilian Salcher, Huseyin Naci, Tyler J. Law, Titus Kuehne, Stephan Schubert, Marcus Kelm, and on behalf of Cardioproof Consortium. Balloon Dilatation and Stenting for Aortic Coarctation: A Systematic Review and Meta-Analysis. *Circulation: Cardiovascular Interventions*, 9(6), June 2016.

[10] Jeffrey Vergales, James Gangemi, Karen Rhueban, and D. Lim. Coarctation of the Aorta - The Current State of Surgical and Transcatheter Therapies. *Current Cardiology Reviews*, 9(3):211–219, August 2013.

[11] Derek Wong, Lee N. Benson, Glen S. Van Arsdell, Tara Karamlou, and Brian W. McCrindle. Balloon angioplasty is preferred to surgery for aortic coarctation. *Cardiology in the Young*, 18(01):79–88, February 2008.

[12] Thomas J. Forbes and Srinath T. Gowda. Intravascular Stent Therapy for Coarctation of the Aorta. *Methodist DeBakey Cardiovascular Journal*, 10(2):82–87, April 2014.

[13] Stephanie Roll, Jacqueline Müller-Nordhorn, Thomas Keil, Hans Scholz, Daniela Eidt, Wolfgang Greiner, and Stefan N Willich. Dacron® vs. PTFE as bypass materials in peripheral vascular surgery – systematic review and meta-analysis. *BMC Surgery*, 8(1):22, December 2008.

[14] Chin Siang Ong, Xun Zhou, Chen Yu Huang, Takuma Fukunishi, Huaitao Zhang, and Narutoshi Hibino. Tissue engineered vascular grafts: current state of the field. *Expert Review of Medical Devices*, 14(5):383–392, May 2017.

[15] Alexandre Joel Chorin. Numerical Solution of the Navier-Stokes Equations. page 18.

[16] Yuji Naito, Toshiharu Shinoka, Daniel Duncan, Narutoshi Hibino, Daniel Solomon, Muriel Cleary, Animesh Rathore, Corey Fein, Spencer Church, and Christopher Breuer. Vascular tissue engineering: Towards the next generation vascular grafts. *Advanced Drug Delivery Reviews*, 63(4-5):312–323, April 2011.

[17] T M Connor and W P Baker. A comparison of coarctation resection and patch angioplasty using postexercise blood pressure measurements. *Circulation*, 64(3):567–572, September 1981.

[18] Matthias Poloczek, Jialei Wang, and Peter I. Frazier. Warm starting Bayesian optimization. In *2016 Winter Simulation Conference (WSC)*, pages 770–781, Washington, DC, USA, December 2016. IEEE.

[19] Saba Mohammadi, Mahdi Mohammadi, Vahab Dehlaghi, and Arash Ahmadi. Automatic Segmentation, Detection, and Diagnosis of Abdominal Aortic

Aneurysm (AAA) Using Convolutional Neural Networks and Hough Circles Algorithm. *Cardiovascular Engineering and Technology*, 10(3):490–499, September 2019.

[20] Seda Aslan, Paige Mass, Yue-Hin Loke, Linnea Warburton, Xiaolong Liu, Narutoshi Hibino, Laura J Olivieri, and Axel Krieger. Non-invasive Prediction of Peak Systolic Pressure Drop across Coarctation of Aorta using Computational Fluid Dynamics. Manuscript submitted for publication. page 4.

[21] Yulei Zhu, Rui Chen, Yu-Hsiang Juan, He Li, Jingjing Wang, Zhuliang Yu, and Hui Liu. Clinical validation and assessment of aortic hemodynamics using computational fluid dynamics simulations from computed tomography angiography. *BioMedical Engineering OnLine*, 17(1):53, December 2018.

[22] Lucian Itu, Puneet Sharma, Kristóf Ralovich, Viorel Mihalef, Razvan Ionasec, Allen Everett, Richard Ringel, Ali Kamen, and Dorin Comaniciu. Non-Invasive Hemodynamic Assessment of Aortic Coarctation: Validation with In Vivo Measurements. *Annals of Biomedical Engineering*, 41(4):669–681, April 2013.

[23] Mirko Bonfanti, Gaia Franzetti, Gabriele Maritati, Shervanthi Homer-Vanniasinkam, Stavroula Balabani, and Vanessa Díaz-Zuccarini. Patient-specific haemodynamic simulations of complex aortic dissections informed by commonly available clinical datasets. *Medical Engineering & Physics*, 71:45–55, September 2019.

[24] S. A. Berger and L-D. Jou. Flows in Stenotic Vessels. *Annual Review of Fluid Mechanics*, 32(1):347–382, January 2000.

[25] Suo Jin, John Oshinski, and Don P. Giddens. Effects of Wall Motion and Compliance on Flow Patterns in the Ascending Aorta. *Journal of Biomechanical Engineering*, 125(3):347–354, June 2003.

[26] Alistair G. Brown, Yubing Shi, Alberto Marzo, Cristina Staicu, Isra Valverde, Philipp Beerbaum, Patricia V. Lawford, and D. Rodney Hose. Accuracy vs. computational time: Translating aortic simulations to the clinic. *Journal of Biomechanics*, 45(3):516–523, February 2012.

[27] Y. d'Udekem, A. J. Iyengar, A. D. Cochrane, L. E. Grigg, J. M. Ramsay, G. R. Wheaton, D. J. Penny, and C. P. Brizard. The Fontan Procedure: Contemporary Techniques Have Improved Long-Term Outcomes. *Circulation*, 116(11):I–157–I–164, September 2007.

[28] Dominik Siallagan, Yue-Hin Loke, Laura Olivieri, Justin Opfermann, Chin Siang Ong, Diane de Zélicourt, Anastasios Petrou, Marianne Schmid Daners, Vartan Kurtcuoglu, Mirko Meboldt, Kevin Nelson, Luca Vricella, Jed Johnson, Narutoshi Hibino, and Axel Krieger. Virtual surgical planning, flow

simulation, and 3-dimensional electrospinning of patient-specific grafts to optimize Fontan hemodynamics. *The Journal of Thoracic and Cardiovascular Surgery*, 155(4):1734–1742, April 2018.

[29] Byeol Kim, Yue-Hin Loke, Florence Stevenson, Dominik Siallagan, Paige Mass, Justin D. Opfermann, Narutoshi Hibino, Laura Olivieri, and Axel Krieger. Virtual Cardiac Surgical Planning Through Hemodynamics Simulation and Design Optimization of Fontan Grafts. In *Medical Image Computing and Computer Assisted Intervention – MICCAI 2019*, volume 11768, pages 200–208, Cham, 2019. Springer International Publishing. Series Title: Lecture Notes in Computer Science.

[30] Jason M. Szafron, Abhay B. Ramachandra, Christopher K. Breuer, Alison L. Marsden, and Jay D. Humphrey. Optimization of Tissue-Engineered Vascular Graft Design Using Computational Modeling. *Tissue Engineering Part C: Methods*, 25(10):561–570, October 2019.

[31] Onur Dur, Sinan Tolga Coskun, Kasim Oguz Coskun, David Frakes, Levent Burak Kara, and Kerem Pekkan. Computer-Aided Patient-Specific Coronary Artery Graft Design Improvements Using CFD Coupled Shape Optimizer. *Cardiovascular Engineering and Technology*, 2(1):35–47, March 2011.

[32] Alfio Quarteroni and Gianluigi Rozza. Optimal control and shape optimization of aorto-coronaric bypass anastomoses. *Mathematical Models and Methods in Applied Sciences*, 13(12):1801–1823, December 2003.

[33] Nikhil Kumar, Anant Diwakar, Sandeep Kumar Attree, and Sanjay Mittal. A method to carry out shape optimization with a large number of design variables. *International Journal for Numerical Methods in Fluids*, 71(12):1494–1508, April 2013.

[34] Joaquim R. R. A. Martins and Andrew B. Lambe. Multidisciplinary Design Optimization: A Survey of Architectures. *AIAA Journal*, 51(9):2049–2075, September 2013.

[35] Valery Agoshkov, Alfio Quarteroni, and Gianluigi Rozza. Shape Design in Aorto-Coronaric Bypass Anastomoses Using Perturbation Theory. *SIAM Journal on Numerical Analysis*, 44(1):367–384, January 2006.

[36] Andrea Manzoni, Alfio Quarteroni, and Gianluigi Rozza. Shape optimization for viscous flows by reduced basis methods and free-form deformation. *International Journal for Numerical Methods in Fluids*, 70(5):646–670, October 2012.

[37] L. E. Carvalho, A. C. Sobieranski, and A. von Wangenheim. 3D Segmentation Algorithms for Computerized Tomographic Imaging: a Systematic Literature Review. *Journal of Digital Imaging*, 31(6):799–850, December 2018.

[38] Won-Keun Kim, Alexander Meyer, Helge Möllmann, Andreas Rolf, Susanne Möllmann, Johannes Blumenstein, Arnaud Van Linden, Christian W. Hamm, Thomas Walther, and Jörg Kempfert. Cyclic changes in area- and perimeter-derived effective dimensions of the aortic annulus measured with multislice computed tomography and comparison with metric intraoperative sizing. *Clinical Research in Cardiology*, 105(7):622–629, July 2016.

[39] Georg Pingen and Kurt Maute. Optimal design for non-Newtonian flows using a topology optimization approach. *Computers & Mathematics with Applications*, 59(7):2340–2350, April 2010.

[40] Bin Zhang and Xiaomin Liu. Topology optimization study of arterial bypass configurations using the level set method. *Structural and Multidisciplinary Optimization*, 51(3):773–798, March 2015.

[41] Luca Antiga, Marina Piccinelli, Lorenzo Botti, Bogdan Ene-Iordache, Andrea Remuzzi, and David A. Steinman. An image-based modeling framework for patient-specific computational hemodynamics. *Medical & Biological Engineering & Computing*, 46(11):1097–1112, November 2008.

[42] Mats Nigam. How to Place Inlet and Outlet Boundary Conditions in CFD Simulations, August 2018.

[43] ANSYS FLUENT Manual. *ANSYS FLUENT Adjoint Solver. Version 19.2. ANSYS*. Ansys, Inc., 2019.

[44] Philippe Reymond, Paolo Crosetto, Simone Deparis, Alfio Quarteroni, and Nikos Stergiopulos. Physiological simulation of blood flow in the aorta: Comparison of hemodynamic indices as predicted by 3-D FSI, 3-D rigid wall and 1-D models. *Medical Engineering & Physics*, 35(6):784–791, June 2013.

[45] ANSYS. ANSYS Fluent - CFD Software | ANSYS, 2019.

[46] Les Peigl. *The NURBS book*. Springer, 2nd edition edition, 1997.

[47] Wei-Liem Loh. On Latin hypercube sampling. *The Annals of Statistics*, 24(5):2058–2080.

[48] Matthias Seeger. Gaussian processes for machine learning. *International Journal of Neural Systems*, 14(2):69–106, 2004.

[49] Ciyou Zhu, Richard H. Byrd, Peihuang Lu, and Jorge Nocedal. Algorithm 778: L-BFGS-B: Fortran subroutines for large-scale bound-constrained optimization. *ACM Transactions on Mathematical Software*, 23(4):550–560, December 1997.

[50] P. Cignoni, C. Rocchini, and R. Scopigno. Metro: Measuring Error on Simplified Surfaces. *Computer Graphics Forum*, 17(2):167–174, June 1998.

[51] M. Probst, M. Lülfesmann, H. M. Bücker, M. Behr, and C. H. Bischof. Sensitivity of shear rate in artificial grafts using automatic differentiation. *International Journal for Numerical Methods in Fluids*, pages 1047–1062, 2009.

[52] Jan Brüning, Florian Hellmeier, Pavlo Yevtushenko, Titus Kühne, and Leonid Goubergrits. Uncertainty Quantification for Non-invasive Assessment of Pressure Drop Across a Coarctation of the Aorta Using CFD. *Cardiovascular Engineering and Technology*, 9(4):582–596, December 2018.

[53] Brent Komer, James Bergstra, and Chris Eliasmith. Hyperopt-Sklearn: Automatic Hyperparameter Configuration for Scikit-Learn. pages 32–37, Austin, Texas, 2014.

[54] Svante Wold, Kim Esbensen, and Paul Geladi. Principal Component Analysis. *Chemometrics and Intelligent Laboratory Systems*, 2:37–52, 1987.

[55] Max A Little, Gael Varoquaux, Sohrab Saeb, Luca Lonini, Arun Jayaraman, David C Mohr, and Konrad P Kording. Using and understanding cross-validation strategies. Perspectives on Saeb et al. *GigaScience*, 6(5), May 2017.

[56] Christodoulos A Floudas. *Nonlinear and Mixed-Integer Optimization*. Oxford University Press, 1995.

[57] M. E. Abbasov and V. F. Demyanov. Proper and adjoint exhausters in nonsmooth analysis: optimality conditions. *Journal of Global Optimization*, 56(2):569–585, June 2013.